Mechanical distribution of the pseudoscalar charmonium and bottomonium on the light-front

Ashutosh Dwibedi,[1,*] Satyajit Puhan,[2,†] and Sabyasachi Ghosh[1,‡]

[1]*Department of Physics, Indian Institute of Technology Bhilai, Kutelabhata, Durg 491002, Chhattisgarh, India*

[2]*Institute of Physics, Academia Sinica, Taipei 11529, Taiwan*

(Received 12 June 2026; accepted 30 September 2026; published 26 October 2026)

We investigate the energy-momentum tensor of pseudoscalar charmonium and bottomonium within the framework of the self-consistent light-front quark model. The gravitational form factors (GFFs), namely the A and D-terms, are evaluated in terms of the light-front wave functions. The corresponding spatial mechanical distributions in the transverse plane are obtained through the Fourier transform of these GFFs. To examine the sensitivity of the results to the internal quark-antiquark distribution inside the meson, two distinct Gaussian forms are employed for the spatial part of the wave function. We analyze several mechanical properties in the transverse plane, including the momentum density, pressure distribution, shear stress, force density, and internal energy density. The pressure distribution exhibits a node where it changes sign from positive (repulsive) to negative (attractive) with increasing transverse distance. The force distribution remains positive throughout the transverse plane, supporting the stability condition proposed in earlier studies. Most of the spatial distributions, except for the shear stress, are found to be sensitive to the choice of the spatial wave function near the center of the meson, while they become nearly insensitive toward the periphery. In contrast, the shear stress distribution exhibits noticeable sensitivity to the choice of wave function in the intermediate transverse region.

DOI: 10.1103/bbm8-c5yj

I. INTRODUCTION

The study of mechanical distributions inside hadrons has recently gained significant attention, particularly following the extraction of the proton pressure from experimental data [1]. The internal pressure and force distributions of hadrons are closely related to the so-called D-term (or D-form factor), also referred to as the Druck term [2,3], which has been described as the "last global unknown" of hadron structure [3]. The electromagnetic form factors (EMFFs) are well established. They are obtained from matrix elements of the electromagnetic current between hadronic states. These form factors encode information about the spatial distributions of charge and current inside hadrons. In contrast, the mechanical properties of hadrons are determined from matrix elements of the energy-momentum tensor (EMT). These matrix elements give rise to gravitational form factors (GFFs), which remain comparatively less explored. The GFFs provide access to fundamental properties of hadrons, including their mass, energy, angular momentum, and internal stress distributions [3,4]. From the experimental perspective, the expected tools to measure GFFs are the hard exclusive processes like the deeply virtual Compton scattering (DVCS) [5], which probes the generalized parton distributions (GPDs) [6–9]. The future Electron-Ion Collider (EIC) [10–12] with its larger kinematic range and high luminosity is expected to significantly advance the experimental determination of GPDs.

While considerable progress has been achieved in understanding the gravitational structure of the nucleons [2,13–44] and pions [39,40,45–55] (also see Ref. [56]), studies of the heavy mesonic sector remain relatively limited [57–59]. In particular, pseudoscalar quarkonia—such as charmonium and bottomonium—offer a unique framework to probe the gravitational structure of hadrons in the heavy-quark sector. Due to the large masses of the constituent quarks, these systems are well-suited for investigating the interplay between nonperturbative QCD dynamics and heavy-quark effects. Therefore, exploring the GFFs of pseudoscalar charmonium and bottomonium states can provide valuable insights into confinement and the internal mechanical properties of heavy hadrons.

Calculation of the GFFs, as well as other quark-quark correlations inside the hadron from the fundamental QCD lagrangian, is a formidable task because of the

*Contact author: ashutoshdwibedi92@gmail.com
†Contact author: puhansatyajit@gmail.com
‡Contact author: sabya@iitbhilai.ac.in

Published by the American Physical Society under the terms of the Creative Commons Attribution 4.0 International license. Further distribution of this work must maintain attribution to the author(s) and the published article's title, journal citation, and DOI. Funded by SCOAP³.

nonperturbative nature of the problem. Low-energy effective models are useful in this respect and have been widely used in studies of hadronic properties [33,45,46,60]. One such model is the light-front constituent quark model (LFQM) [60]. In LFQM, a meson state is expanded in the Fock basis containing the valence quark-antiquark pair as well as sea quarks and gluons. In the model scale (taken as of the order of the mass of the constituent quarks), it is customary to truncate these infinitely many Fock terms into the valence sector consisting of only a valence quark-antiquark pair. In this valence Fock state approximation, the meson states can be expressed as a two-body light-front wave function (LFWF) consisting of relative momenta of the quark-antiquark pair and their helicities. The hadronic properties are then readily obtained as the overlap of the LFWFs. In the LFQM, GFFs are expressed as the matrix element of the hadronic EMT tensor and subsequently expressed as the overlap integrals of LFWFs. However, it is worth noting that evaluating the D-term in this approach poses a considerable challenge, as it inevitably involves the so-called "bad" current components, which are sensitive to LF zero modes [61]. Over the years, a self-consistent LFQM has been developed that successfully addresses this zero-mode contamination in light-front (LF) dynamics in a variety of hadronic observables [61–68]. This approach gives a way of calculating physical observables in a current-component independent manner (including the "bad" current components), which are otherwise hindered in standard LFQM. Within this approach, in particular, Ref. [66] obtained the pseudoscalar and vector meson decay constants in a current-component- and polarization-independent manner. In Refs. [62,63], it has been discussed how this approach is consistent with the chiral symmetry of QCD in the context of pion and kaon distribution amplitudes and EMFFs. More recently, the EMFFs [68] and GFFs [55] of the pion were calculated within this approach, demonstrating the independence of the extracted form factors from the choice of current component. This approach, in particular, is applicable to symmetric-mass mesons, and it is followed here to extract the GFFs of η_c and η_b.

In the present work, we calculate the GFFs, i.e., A and D-terms of the η_c and η_b mesons by evaluating the matrix element of the EMT operator containing only the noninteracting quark fields. Various spatial mechanical distributions in the transverse plane are related to the Fourier transforms of these GFFs. We define these distributions in a completely relativistically invariant way, respecting the uncertainty principle, following the Refs. [21,69–71]. These distributions are subsequently evaluated in the transverse plane at a constant LF time. In particular, we determine the longitudinal momentum density, pressure distribution, shear stresses, force distribution, and internal energy distribution in the transverse plane. To check the sensitivity of the results on the quark-antiquark distribution inside the mesons, we use two sets of spatial wave functions in the present work, differing by the so-called "Jacobi factor" [72,73].

The present work is organized as follows. In Secs. II A—II C, we present the LFQM framework, the evaluation of the GFFs within the LFQM, and the spatial distributions inside the mesons, respectively. Section III contains the numerical results for the GFFs and the corresponding spatial distributions obtained using two different choices of wave functions. Finally, we summarize our findings and conclude in Sec. IV. Additional details and intermediate derivations are provided in Appendixes A–D. Appendix A covers the LF conventions and spinors, Appendix B the EMT matrix elements, Appendix C the BT construction and equivalent GFF expressions, and Appendix D the associated spatial densities and useful formulas.

II. FORMALISM

A. Description of pseudoscalar quarkonia in light-front quark model

We begin by describing the valence Fock sector of scalar quarkonia ($Q\bar{Q}$) in the LFQM. At fixed LF time $z^+ = t + z = 0$ [74], the valence Fock state $|Q\bar{Q}(x_i P^+, \vec{k}_{\perp i} + x_i \vec{P}_\perp, \lambda_i)\rangle$ for a pseudoscalar quarkonium with total four-momentum $P^\mu \equiv P = (P^+, \vec{P}_\perp, P^-)$ is expressed in terms of the internal variables $x_i = \frac{k_i^+}{P^+}$, $\vec{k}_{\perp i}$, and λ_i, which represent the boost-invariant longitudinal momentum fraction, transverse internal momentum, and helicity carried by the ith constituent parton, respectively.[1] These variables satisfy the momentum-conservation conditions $\sum_i x_i = 1$ and $\sum_i \vec{k}_{\perp i} = 0$. The valence state of the quarkonium is expressed as

$$|\mathcal{M}(P^+, \vec{P}_\perp)\rangle = \sum_{\lambda_q, \lambda_{\bar{q}}} \int \frac{dx_q dx_{\bar{q}} d^2\vec{k}_{q\perp} d^2\vec{k}_{\bar{q}\perp}}{2(2\pi)^3 2(2\pi)^3 \sqrt{x_q x_{\bar{q}}}} 2(2\pi)^3 \delta(1 - x_q - x_{\bar{q}}) \delta^2(\vec{k}_{q\perp} + \vec{k}_{\bar{q}\perp}) \Psi(x_q, x_{\bar{q}}, \vec{k}_{q\perp}, \vec{k}_{\bar{q}\perp}, \lambda_q, \lambda_{\bar{q}})$$
$$\times |x_q P^+, x_{\bar{q}} P^+, x_q \vec{P}_\perp + \vec{k}_{q\perp}, x_{\bar{q}} \vec{P}_\perp + \vec{k}_{\bar{q}\perp} \lambda_q, \lambda_{\bar{q}}\rangle$$

where the subscripts q and $\bar{q}$ are used for the quark and antiquark, respectively. Simplifying the above integral by integrating over $x_{\bar{q}}$ and $\vec{k}_{\bar{q}\perp}$ we have

[1]The index i in our case would belongs to either $(c, \bar{c})$ for charmonium or $(b, \bar{b})$ for bottomonium. We generically call them $(q, \bar{q})$.

$$|\mathcal{M}(P^+,\vec{P}_\perp)\rangle = \sum_{\lambda_q,\lambda_{\bar{q}}} \int \frac{dxd^2\mathbf{k}_\perp}{16\pi^3\sqrt{x(1-x)}} \Psi(x,\vec{k}_\perp,\lambda_q,\lambda_{\bar{q}})|xP^+,\vec{k}_\perp,\lambda_q,\lambda_{\bar{q}}\rangle. \tag{1}$$

where we redefine

$$x_q \equiv x, \vec{k}_{q\perp} \equiv \vec{k}_\perp \quad \text{and} \quad |x_qP^+,(1-x_q)P^+,x_q\vec{P}_\perp+\vec{k}_{q\perp},(1-x_q)\vec{P}_\perp-\vec{k}_{q\perp},\lambda_q,\lambda_{\bar{q}}\rangle \equiv |x_qP^+,x_q\vec{P}_\perp+\vec{k}_{q\perp},\lambda_q,\lambda_{\bar{q}}\rangle.$$

The quark and anti quark momentum can be identified as: $\vec{p}_q = (p_q^+ \equiv x_qP^+, \vec{p}_{q\perp} \equiv x_q\vec{P}_\perp + \vec{k}_{q\perp})$ and $\vec{p}_{\bar{q}} = (p_{\bar{q}}^+ \equiv x_{\bar{q}}P^+, \vec{p}_{\bar{q}\perp} \equiv x_{\bar{q}}\vec{P}_\perp + \vec{k}_{\bar{q}\perp})$. The total wave function Ψ is written as a product of the space wave function φ and spin wave function $\mathcal{S}$, i.e., $\Psi(x,\vec{k}_\perp,\lambda_q,\lambda_{\bar{q}}) = \varphi(x,\vec{k}_\perp)\mathcal{S}_{\lambda_q\lambda_{\bar{q}}}(x,\vec{k}_\perp)$. The spin wave functions are obtained from the instant from spin states via Melosh-Wigner transformation [75,76] or equivalently by the choice of the appropriate quark-meson vertex [77]

$$\mathcal{S}_{\lambda_q\lambda_{\bar{q}}} = \frac{1}{\sqrt{2}M_0}\bar{u}_{\lambda_q}(p_q)\gamma_5\, v_{\lambda_{\bar{q}}}(p_{\bar{q}}), \quad \text{where } M_0^2 = \frac{\vec{k}_\perp^2+m_q^2}{x(1-x)} \tag{2}$$

is the squared invariant mass of the quarkonium. The detailed form of the spin wave functions along with the definitions of the LF spinors are provided in Appendix A. The instant form momentum space wave function in the quarkonium rest frame or center-of-momentum (CM) frame can be assumed to be of the harmonic oscillator form, i.e.,

$$\varphi^{\rm CM} = \frac{1}{\pi^{3/4}\beta^{3/2}} e^{-(\vec{p}^{\rm CM})^2/2\beta^2}, \tag{3}$$

where β is the harmonic scale parameter determining the width of the wave function. In order to obtain the momentum-space wave function in the front form, $\varphi(x,\vec{k}_\perp)$, from the CM frame wave function in the instant form, $\varphi^{\rm CM}(\vec{p}^{\rm CM})$, one employs the Brodsky-Huang-Lepage (BHL) prescription [78–80]. According to this prescription, the correspondence between the CM and LF momentum variables is given by $\vec{p}_\perp^{\rm CM} = \vec{k}_\perp$ and $p_z^{\rm CM} = (x-\frac{1}{2})M_0$. Therefore, in the BHL prescription, we have

$$\varphi(x,\vec{k}_\perp) \propto \varphi_{\rm CM}\left((\vec{p}^{\rm CM})^2 = \frac{\vec{k}_\perp^2+m_q^2}{4x(1-x)} - m_q^2\right). \tag{4}$$

In the current paper, two sets of momentum-space wave functions have been chosen for analysis, which mainly differ from $\varphi_{\rm CM}$ by a product of $(x,\vec{k}_\perp)$ dependent factor (known as the "Jacobi factor" [72,73]). The first set we use has been abundantly used in the LFQM studies of heavy mesons [60,77,81,82]

$$\begin{aligned}\varphi^{\rm CJ}(x,\vec{k}_\perp) &= \frac{\sqrt{2(2\pi)^3}}{\pi^{3/4}\beta^{3/2}}\sqrt{\frac{\partial p_z^{\rm CM}}{\partial x}}\exp\left[\frac{m_q^2}{2\beta^2}\right] \\ &\quad\times\exp\left[-\frac{m_q^2+\vec{k}_\perp^2}{8x(1-x)\beta^2}\right] \\ &= \frac{\sqrt{2(2\pi)^3}}{\pi^{3/4}\beta^{3/2}}\sqrt{\frac{M_0}{4x(1-x)}}\exp\left[\frac{m_q^2}{2\beta^2}\right] \\ &\quad\times\exp\left[-\frac{m_q^2+\vec{k}_\perp^2}{8x(1-x)\beta^2}\right], ({\rm SET-I}).\end{aligned} \tag{5}$$

This form was introduced by Chung-Coester-Polyzou [81] and has been extensively used by C.R. Ji and collaborators [83–89] to describe the properties of hadrons in LF models. The Jacobian factor $M_0/4x(1-x)$ comes from relating the instant form differentials $d^3\vec{p}^{\rm CM}$ to $d^2\vec{k}_\perp dx$. Another set which we use is introduced in Refs. [90,91] and further used in the LF analysis [72] (also see the review [92]),

$$\begin{aligned}\varphi^{\rm TK}(x,\vec{k}_\perp) &= A_{\rm TK}\sqrt{\frac{1}{2x(1-x)}}\exp\left[\frac{m_q^2}{2\beta^2}\right] \\ &\quad\times\exp\left[-\frac{m_q^2+\vec{k}_\perp^2}{8x(1-x)\beta^2}\right], ({\rm SET-II}).\end{aligned} \tag{6}$$

The jacobian factor $1/2x(1-x)$ in Eq. (6) comes from relating the instant form differentials $d^3\vec{p}^{\rm CM}/p_0^{\rm CM}$ to $d^2\vec{k}_\perp dx$.

One can observe that the spin wave functions in Eq. (A10) satisfy the following normalization relation,

$$\sum_{\lambda_q\lambda_{\bar{q}}} \mathcal{S}^*_{\lambda_q\lambda_{\bar{q}}}(x,\vec{k}_\perp)\mathcal{S}_{\lambda_q\lambda_{\bar{q}}}(x,\vec{k}_\perp) = 1. \tag{7}$$

Since the total wave function (space and spin) has to be normalized, this gives the following normalization condition for the space part of the wave function:

$$\begin{aligned}&\sum_{\lambda_q\lambda_{\bar{q}}}\int\frac{dxd^2\vec{k}_\perp}{2(2\pi)^3}\Psi^*(x,\vec{k}_\perp,\lambda_q,\lambda_{\bar{q}})\Psi(x,\vec{k}_\perp,\lambda_q,\lambda_{\bar{q}}) \\ &= \int\frac{dxd^2\vec{k}_\perp}{2(2\pi)^3}|\varphi(x,\vec{k}_\perp)|^2 = 1.\end{aligned} \tag{8}$$

B. Gravitational form factors in the self-consistent light-front quark model

We consider a process in which a pseudoscalar quarkonia undergoes a transition from an initial state with momentum P to a final state with momentum P'. The GFF of the quakonia can be obtained from the expression of the following matrix element of the EMT operator [55]:

$$T^{\mu\nu} \equiv \langle \hat{T}^{\mu\nu}(0) \rangle = \langle \mathcal{M}(P')|\hat{T}^{\mu\nu}(0)|\mathcal{M}(P)\rangle, \tag{9}$$

where $|\mathcal{M}(P)\rangle$ and $|\mathcal{M}(P')\rangle$ correspond to initial and final state of the meson. For our purpose, we choose the following form of the EMT operator, ignoring the gluon gauge fields [55]

$$\hat{T}^{\mu\nu} = \frac{1}{4}\bar{\psi}_q(z)(i\gamma^\mu \overleftrightarrow{\partial}^\nu + i\gamma^\nu \overleftrightarrow{\partial}^\mu)\psi_q(z), \tag{10}$$

where, q stands for either charm (c) or bottom (b). Lorentz symmetry gives the decomposition of the matrix element containing Lorentz structures and the corresponding GFF [3,55],

$$T^{\mu\nu} = A\Gamma_A^{\mu\nu} + D\Gamma_D^{\mu\nu}, \tag{11}$$

where A describes the quark and antiquark contribution to the energy and momentum densities, while D characterizes the quark and antiquark contribution to the internal pressure and shear stress distributions. Both the A and D-terms can be written down as a sum of quark and antiquark contributions as $A = A_q + A_{\bar{q}}$ and $D = D_q + D_{\bar{q}}$. One usually expresses the Lorentz structure with the help of the average momentum $\bar{P} = \frac{P+P'}{2}$ and momentum transfer $\Delta = P' - P$ as, $\Gamma_A^{\mu\nu} = 2\bar{P}^\mu\bar{P}^\nu$ and $\Gamma_D^{\mu\nu} = \frac{1}{2}(\Delta^\mu\Delta^\nu - g^{\mu\nu}\Delta^2)$.

It is noteworthy that, while Eq. (11) provides the Lorentz decomposition of the matrix elements of the physical EMT and preserves complete Poincaré symmetry, a practical model calculation does not necessarily retain this property [91]. In practice, the left-hand side of Eq. (11) is evaluated within LF dynamics using a suitable QCD-motivated model, typically with a truncated Fock space. In the LFQM considered in Sec. II A, for example, we restrict the Fock space to the valence sector. Such a truncation can give rise to several issues that require careful consideration, including zero-mode contributions [93], violation of Lorentz covariance [91], and frame dependence [94]. These issues are not unique to the calculation of GFFs, but also arise in the evaluation of other partonic observables, such as distribution amplitudes [61] and EMFF [62]. A common strategy for mitigating these issues in LF approaches is to identify the so-called "good components" of the relevant currents and use them to extract the physical observables. Accordingly, the identification of the good current components and the characterization of spurious contributions associated with the "bad components" have been investigated for various partonic observables. In particular, to account for the loss of Lorentz covariance in LF calculations, a lightlike four-vector ω can be introduced into the Lorentz decomposition of the hadronic matrix element [91,95]. Its presence allows the genuine Lorentz structures, and hence the physical form factors, to be distinguished from spurious contributions induced by the LF formulation. For the hadronic EMT, this issue has been investigated in Refs. [96–98], where the appropriate current components for extracting the physical form factors and isolating the spurious contributions were identified within a strongly coupled scalar theory in the LF Hamiltonian formalism.

A complementary approach to the treatment of spurious contributions was developed by Jaus [93], who established a connection between covariant Bethe-Salpeter calculations and LFQMs. This framework was subsequently modified and extended by Choi and Ji [61–65] and further developed in Refs. [66–68]. In this approach, the LF vertex function obtained in the covariant Bethe-Salpeter approach was mapped onto a typical Gaussian trial wave function, with a consistent replacement of the meson mass by its invariant mass. A remarkable finding of this analysis was that both the zero-mode and instantaneous contributions, which are present in the covariant Bethe-Salpeter model, are absent in the LFQM when the constituent quark and antiquark are treated as LF on-mass-shell degrees of freedom. Readers interested in the details of the method are referred to the original works [61–68], which collectively establish the framework known as the self-consistent LFQM to obtain the physical observables in a manner independent of the current components. In what follows, we briefly describe this method and discuss the extraction of the GFFs of quarkonia within this framework.

In the standard LFQM described in Sec. II A, one describes the meson state in a noninteracting $Q\bar{Q}$ Fock state. As a result, the total four momentum $P = p_q + p_{\bar{q}}$ is required to be conserved at a meson-quark vertex. In particular, the LF energy conservation $P^- = p_q^- + p_{\bar{q}}^-, \Rightarrow \frac{M_0^2+\vec{P}_\perp^2}{P^+} = \frac{m_q^2+\vec{p}_{q\perp}^2}{p_q^+} + \frac{m_{\bar{q}}^2+\vec{p}_{\bar{q}\perp}^2}{p_{\bar{q}}^+}$ necessitate the use of invariant mass M_0 in place of the physical meson mass M in a meson-quark vertex [68]. In accordance with this, the spin wave function is obtained by interaction-independent Melosh rotation of on-mass-shell quarks and antiquarks. One can notice that the spin wave function as specified in Eq. (2) contains the invariant mass of the system M_0 and is automatically normalized [see Eq. (7)]. The effect of interaction is introduced only in the mass operator M through the phenomenological $V_{Q\bar{Q}}$ potential [99], i.e., $M = M_0 + V_{Q\bar{Q}}$ to be consistent with the Bakamjian-Thomas (BT) construction [100,101] and preserve the group structure or the commutation relation of the operators. The interaction in turn fixes the radial wave function

parameters, m_q and β through variational analysis [60,86,102,103].

The traditional LFQMs [77,104,105] use BT construction (the replacement $M \to M_0$) only in evaluating the matrix element, e.g., on Eq. (9) or the left-hand side of Eq. (11), while leaving the Lorentz structure [right-hand side of Eq. (11)] intact. The selective application of BT construction only to the matrix elements yields LF zero modes that affect physical observables [55,61–68]. This results in different values for the same observables when extracted from different current components (particularly when "bad current components" are used). We have demonstrated this fact, in connection with EMT, in Appendix C [see Eqs. (C9)–(C15)]. Therefore, it is also important to apply the BT construction to both the Lorentz factors and matrix elements [55,61–68] to realize a consistent application of the BT construction up to the level of computation. The consistent application of BT construction within LFQM yields a self-consistent LFQM that can extract physical observables in a current-component-independent manner, including the so-called "bad components." As noted in Ref. [55], the Lorentz structure $\Gamma_A^{\mu\nu}$ must be modified to properly implement the BT construction in LFQM studies, and the physical meson mass M should be replaced with the invariant mass M_0 within both the Lorentz structures $\Gamma_A^{\mu\nu}$ and $\Gamma_D^{\mu\nu}$. Following Ref. [55], we modify the form of Lorentz structure $\Gamma_A^{\mu\nu}$ as $\Gamma_A^{\mu\nu} = 2[\bar{P}^\mu \bar{P}^\nu - \frac{\bar{P}\cdot\Delta}{\Delta^2}(\Delta^\mu \bar{P}^\nu + \Delta^\nu \bar{P}^\mu - \bar{P}\cdot\Delta g^{\mu\nu})]$. Within the BT framework, the invariant masses of the initial and final quarkonia entering the Lorentz structure are generally different, i.e., $M_0^2 \neq M_0'^2 = \frac{\vec{k}_\perp'^2 + m_q^2}{x(1-x)}$. Keeping this in mind, the different components of the Lorentz structures in the BT framework can be worked out easily and are provided in Table III of Appendix C. The extraction of the GFFs of quarkonia in the self-consistent LFQM from different current components is illustrated in detail in Appendix C. Particularly, we numerically establish in Appendix C that different ways (using $++, +i, -i, ij$-EMT components[2] and two different radial wave functions, CJ and TK) of extracting the GFFs lead to the same result in self-consistent LFQM, while the traditional LFQM results predict different values when different current components are used.

For the sake of illustration, we write the following expression for A_q and D_q extracted from $(++)$ and $(+-)$ components using Eq. (9) along with Eq. (11),

$$A_q = \left\langle \frac{T_q^{++}}{\Gamma_A^{++}} \right\rangle_{\rm BT} \tag{12}$$

$$D_q = \left\langle \frac{\Gamma_A^{++} T_q^{+-} - \Gamma_A^{+-} T_q^{++}}{\Gamma_D^{+-} \Gamma_A^{++}} \right\rangle_{\rm BT}. \tag{13}$$

As emphasized in the Appendix C, the Lorentz structures, which now depend on the internal quark momenta, have to be integrated along with the matrix element T_q^{++} and T_q^{++} in the self-consistent LFQM. We provide the details of the evaluation of the matrix element of $T_q^{\mu\nu}$ in the Appendix B. Here, we briefly outline the steps needed to get the final expression for GFFs. The individual meson momentum in terms of the average momentum and momentum transfer is given by $P = \bar{P} - \frac{\Delta}{2}$ and $P' = \bar{P} + \frac{\Delta}{2}$. We would select an asymmetric frame with zero skewness (no longitudinal momentum transfer $\Delta^+ = 0$). The choice of the frame render us with $P'^+ = P^+ = \bar{P}^+$, $\vec{P} = (P^+, \vec{0})$, $\vec{P}' = (P^+, \vec{\Delta}_\perp)$, and $\vec{\bar{P}} = (P^+, \frac{\vec{\Delta}_\perp}{2})$.

The GFFs of the quarkonia can be obtained by calculating the matrix element of the EMT operator and substituting in the expressions (12) and (13). It is worth mentioning that being a symmetric mass system, both the quark and antiquark contribute equally to the GFFs, i.e., $A = 2A_q$ and $D = 2D_q$ (see Appendix B 2 for a formal derivation). The matrix element of the EMT operator can be expressed as

$$\begin{aligned} T_q^{\mu\nu} &\equiv \langle \hat{T}_q^{\mu\nu}(0) \rangle = \langle \mathcal{M}(P') | \hat{T}_q^{\mu\nu}(0) | \mathcal{M}(P) \rangle \\ &= \int \frac{dx d^2\vec{k}_\perp}{2(2\pi)^3} \varphi^*(x, \vec{k}_\perp') \varphi(x, \vec{k}_\perp) \mathrm{Tr}[\mathcal{S}\mathcal{S}'^\dagger U^{\mu\nu}], \end{aligned} \tag{14}$$

where $\mathcal{S}(x, \vec{k}_\perp)$ and $\mathcal{S}' \equiv \mathcal{S}(x, \vec{k}_\perp')$ are the 2×2 matrices (in the helicity space) representing the initial and final state spin wave functions of the quarkonia. $U^{\mu\nu} \equiv U^{\mu\nu}_{\lambda_q' \lambda_q} = \frac{1}{4x} \bar{u}_{\lambda_q'}(p_q')[\gamma^\mu p_{sq}^\nu + \gamma^\nu p_{sq}^\mu] u_{\lambda_q}(p_q)$ is a specific Dirac structure which determines the spin trace of the tensor current $S_q^{\mu\nu} \equiv \mathrm{Tr}[\mathcal{S}\mathcal{S}'^\dagger U^{\mu\nu}]$.[3] The momentum variables of the LF Dirac spinors occurring in the definition of the $U^{\mu\nu}$ represent the momentum of the active quark. The momenta of the incoming quark and the outgoing quark are, respectively, $p_q = (p_q^-, p_q^+, \vec{p}_{q\perp}) = (\frac{\vec{p}_{q\perp}^2 + m_q^2}{p_q^+}, xP^+, \vec{k}_\perp)$ and $p_q' = (p_q'^-, p_q'^+, \vec{p}_{q\perp}') = (\frac{\vec{p}_{q\perp}'^2 + m_q^2}{p_q'^+}, xP^+, x\vec{P}_\perp' + \vec{k}_\perp')$. As the momentum of the spectator antiquark remains unchanged, we have $\vec{k}_\perp + \vec{\Delta}_\perp = x\vec{P}_\perp' + \vec{k}_\perp'$ which implies $\vec{k}_\perp' = \vec{k}_\perp + (1-x)\vec{\Delta}_\perp$. The total quark momentum is denoted by $p_{sq} = p_q + p_q'$.

C. Distributions in transverse plane

The distribution of the spatial densities inside the hadrons, as the Fourier transformation of the corresponding

[2]We also see that $(--)$-EMT component leads to different results in the self-consistent LFQM as found in Ref. [55] for pion and should be discarded in studying the GFFs within the present framework.

[3]While the spin indices (λ) are explicitly shown in the derivation provided in the Appendix, here we are only keeping the Dirac indices and ignoring the helicity or the spin indices.

form factors, is tempting, and, in fact, has been defined in this way in the past. In this definition, one takes a 3D Fourier transformation of the form factors in the Breit frame $\bar{P} = (E, 0, 0, 0)$ and obtains the full 3D instant form spatial densities of the hadron [3,106]. However, as pointed out in several references [107–109], these densities suffer from relativistic and quantum delocalization effects [109]. Properly defined 3D densities can be obtained in the full nonrelativistic limits as mentioned in the Ref. [70]. However, this field is active, and readers can consult Ref. [110] for further discussion.

In this section, we discuss the transverse plane 2D densities obtained in the LF formalism, which are fully consistent with relativity. These 2D distributions for the EMT were introduced in Ref. [18] in the Wigner function formalism and later confirmed in Refs. [21,69–71]. We follow the Refs. [21,69–71] where the LF 2D density have been defined as the expectation value of the relevant operator in a localized hadron state (spatially localized in the transverse plane). In Refs. [21,69–71], starting from the expectation value of the EMT operator in a localized wave function, the authors have shown that the internal momentum, stress, and energy distribution can be obtained from the 2D Fourier transformation of the matrix element of the EMT operator. Appendix D contains a brief discussion along these lines, along with derivations of some useful formulas to which readers may refer. Once the A and D-terms of the quarkonia are known one can express the matrix element of the EMT as

$$T^{\mu\nu} = 2\bar{P}^{\mu}\bar{P}^{\nu}A + \frac{\Delta^{\mu}\Delta^{\nu} - g^{\mu\nu}\Delta^2}{2}D. \tag{15}$$

The pure stress tensor is associated with the following Fourier transformation,

$$S^{ij} = \frac{1}{4P^+}\int \frac{d^2\vec{\Delta}_\perp}{(2\pi)^2} e^{-i\vec{\Delta}_\perp\cdot\vec{z}_\perp}(\Delta^i_\perp\Delta^j_\perp - \vec{\Delta}^2_\perp\delta^{ij})D(-\vec{\Delta}^2_\perp). \tag{16}$$

While the pure stress tensor is dependent on the state of the quarkonia via P^+, an internal stress tensor defined by $\mathcal{S}^{ij} \equiv P^+S^{ij}$ is not. Drawing an analogy from continuum mechanics, we can define the pure stress tensor as the decomposition,

$$S^{ij} = \left(\frac{z^i_\perp z^j_\perp}{z^2_\perp} - \frac{1}{2}\delta^{ij}\right)s(z_\perp) + \delta^{ij}p(z_\perp), \tag{17}$$

where p and s are the LF static pressure and shear function (give rise to shear stresses), respectively, with $|\vec{z}_\perp| = z_\perp$ is the distance in the transverse plane. The shear function and pressure can be obtained by comparing the fundamental definition (16) with the tensor decomposition (17) as (see Appendix D),

$$s(z_\perp) = -z_\perp\frac{d}{dz_\perp}\left(\frac{1}{z_\perp}\frac{d\tilde{D}}{dz_\perp}\right), \tag{18}$$

$$p(z_\perp) = \frac{1}{2z_\perp}\frac{d}{dz_\perp}\left(z_\perp\frac{d\tilde{D}}{dz_\perp}\right), \tag{19}$$

$$\text{where } \tilde{D} \equiv \frac{1}{4P^+}\int\frac{d^2\vec{\Delta}_\perp}{(2\pi)^2}e^{-i\vec{\Delta}_\perp\cdot\vec{z}_\perp}D(-\vec{\Delta}^2_\perp). \tag{20}$$

By virtue of the relation obtained above and EMT conservation, the shear function and pressure obey certain conditions [69],

$$\frac{dp(z_\perp)}{dz_\perp} + \frac{1}{z_\perp}s(z_\perp) + \frac{1}{2}\frac{ds(z_\perp)}{dz_\perp} = 0 \tag{21}$$

$$\text{and} \quad \int d^2\vec{z}_\perp p(z_\perp) = 0. \tag{22}$$

Equation (21) is a direct result of $\partial_i S^{ij} = 0$, whereas the second equality (22), known as the von Laue condition of stability, is an implication of the expression of the pressure stated in Eq. (19). The effective normal force density on a 1D surface[4] is obtained as $\mathcal{F}^i = S^{ij}n^j = \frac{z^j_\perp}{z_\perp}(p + \frac{1}{2}s)$, where n^j is the normal to the surface. Apart from the von Laue global stability condition, the local stability of the matter implies an outward force at any point [69,111], i.e., $p + \frac{1}{2}s > 0$. One defines the LF momentum (P^+) and energy (P^-) densities in a similar manner as [71]

$$\mathcal{P} = P^+\int\frac{d^2\vec{\Delta}_\perp}{(2\pi)^2}e^{-i\vec{\Delta}_\perp\cdot\vec{z}_\perp}A(-\vec{\Delta}^2_\perp) \tag{23}$$

$$\mathcal{E} = \frac{1}{2P^+}\int\frac{d^2\vec{\Delta}_\perp}{(2\pi)^2}e^{-i\vec{\Delta}_\perp\cdot\vec{z}_\perp}\left(\left(M^2 + \frac{\vec{\Delta}^2_\perp}{4}\right)\times A(-\vec{\Delta}^2_\perp) + \frac{\vec{\Delta}^2_\perp}{2}D(-\vec{\Delta}^2_\perp)\right). \tag{24}$$

The mean squared radius associated with momentum and force is given by

$$\langle z^2_\perp\rangle_{\mathcal{P}} = \frac{1}{P^+}\int d^2\vec{z}_\perp z^2_\perp\mathcal{P}(z_\perp) \tag{25}$$

$$\langle z^2_\perp\rangle_{\mathscr{F}} = \frac{\int d^2\vec{z}_\perp z^2_\perp(p(z_\perp) + \frac{1}{2}s(z_\perp))}{\int d^2\vec{z}_\perp(p(z_\perp) + \frac{1}{2}s(z_\perp))}. \tag{26}$$

[4]This is basically a line in 2D. We choose it to be a circular section.

III. RESULTS AND DISCUSSIONS

In this section, we describe the results of the GFFs and the corresponding spatial densities in the transverse plane using the expressions provided in Secs. II B and II C. Specifically, for A_q and D_q-terms, we use Eqs. (12) and (13), respectively, where the components of the EMT tensor given in Eq. (14) are evaluated using the spin trace of the tensor current provided in Table II. Two different sets of wave functions, i.e., SET-I corresponding to $\varphi^{\rm CJ}$ (Eq. (5) and SET-II corresponding to $\varphi^{\rm TK}$ [Eq. (6)], are used for each result. It should be noted that the wave functions are characterized by two parameters, the mass of the quark (or antiquark) m_q and the harmonic parameter β. In the following results and discussion, we use a common set of parameters for both wave functions to isolate the differences arising from their shapes. The parameters are adopted from Ref. [102]: $m_c = 1.68$ GeV, $m_b = 5.10$ GeV, $\beta_{\eta_c} = 0.699$ GeV and $\beta_{\eta_b} = 1.376$ GeV.

To begin with, we display the A-term as a function of the momentum transfer. From Fig. 1, we observe that $A(-\vec{\Delta}_\perp^2)$ satisfies the momentum sum rule [69], namely $A(0) = 1$, for both charmonium and bottomonium. We also find that the A-term decreases with increasing momentum transfer for both quarkonia. For charmonium, a clear difference between the results obtained from different wave functions appears at high momentum transfer. In contrast, this difference is only marginal for bottomonium. The slope of the momentum form factor at zero momentum transfer provides a measure of the longitudinal momentum distribution in the transverse plane [69] (We discuss more regarding this at the end of this section, also see Eq. (D15) of Appendix D). From the slopes shown in Fig. 1, it is evident that the longitudinal momentum in bottomonium is distributed over a smaller transverse area compared to charmonium.

In Fig. 2, we display the so-called Druck term or D-term for quarkonia. Unlike the A-term, there are no established

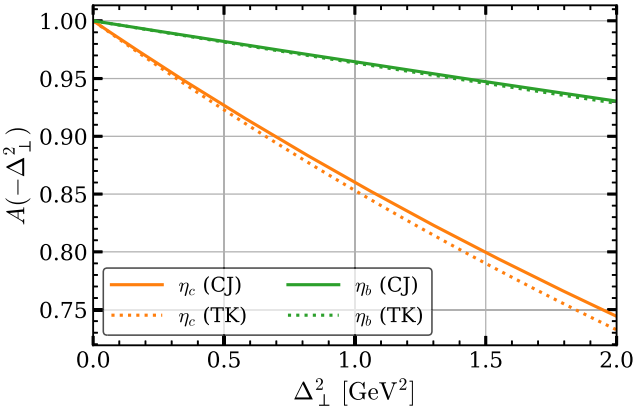


FIG. 1. Variation of the A-term with squared momentum transfer.

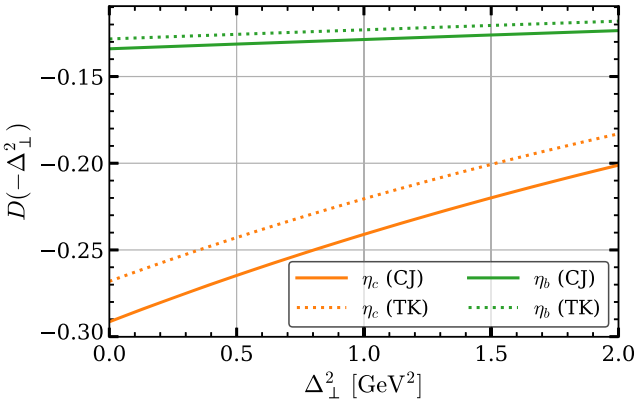


FIG. 2. Variation of the D-term with squared momentum transfer.

values or constraints for the magnitude of the D-term at zero momentum transfer except for the pion. For the pion, low-energy theorems can be used to dictate the value to be -1 in the chiral limit, i.e., $D_\pi(-\vec{\Delta}_\perp^2 = 0) = -1$ for $m_\pi \to 0$ with corrections terms at finite pion mass (See Ref. [112] and also articles cited there in). For heavy mesons made up of heavy quarks, the magnitude of $D(-\vec{\Delta}_\perp^2 = 0)$ can be different from one while still staying negative. We notice in Fig. 2 that the magnitude of the $D(-\vec{\Delta}_\perp^2 = 0)$ is far from the value -1 predicted for the Goldstone bosons. For bottomonium, which is heavier than for charmonium, the value of $D_\pi(-\vec{\Delta}_\perp^2 = 0)$ is even farther away from -1. Our results for the D-term are found to be consistent with the contact-interaction approach [57], while they deviate from the results reported in Refs. [58,59]. At zero transverse momentum transfer, we observe the $D(-\vec{\Delta}_\perp^2 = 0)$ values are obtained as

$$D_{\eta_c}^{\rm CJ} = -0.291, \qquad D_{\eta_b}^{\rm CJ} = -0.134,$$
$$D_{\eta_c}^{\rm TK} = -0.268, \qquad D_{\eta_b}^{\rm TK} = -0.127. \tag{27}$$

We also see a clear dependence of the space wave function on the behavior of the D as a function of momentum transfer. The magnitude of the D decreases as the momentum transfer increases for both the quarkonia, and the wave function dependence is pronounced for η_c than η_b.

For completeness, we also show the EMFFs of the quarkonia as a function of momentum transfer in Fig. 3 as well as a unified comparison in Fig. 4 for both the choices of wave functions. The expression of the EMFF in terms of an integral over the LFWFs is well established and can be found in Refs. [113,114]. We notice a slight variation of the EMFF with the wave function for the case of η_c and marginal variations in η_b. We compare our results for the EMFF with lattice simulations for the meson η_c. Our results are in good agreement with the lattice data of the Refs. [115–117]. In Fig. 4 we present all the form factors

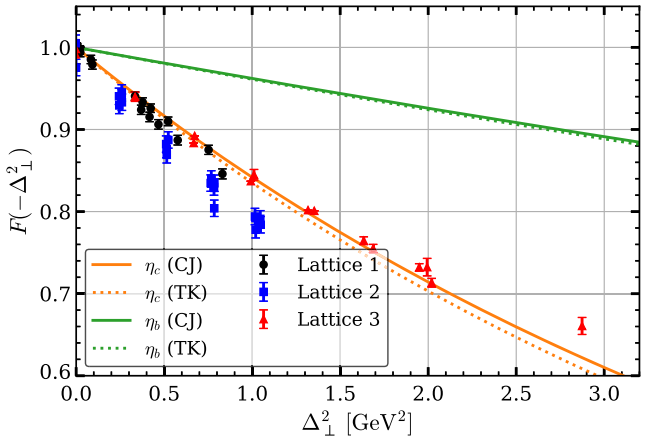


FIG. 3. Variation of the EMFFs with squared momentum transfer. For the case of η_c the data points of lattice 1 [115], 2 [116], and 3 [117] are also put for comparison.

as a function of momentum transfer. This shows nicely all the form factors relative momentum dependence as well as the dependence on the spatial wave functions. The normalized value of the D-term, i.e., $D/D(0)$ as a function of momentum transfer, provides a measure of force

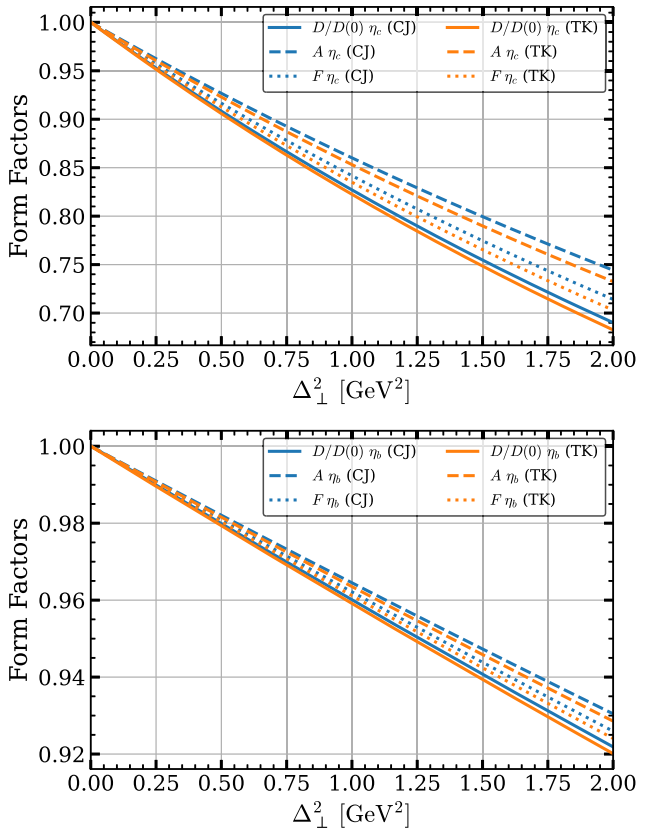
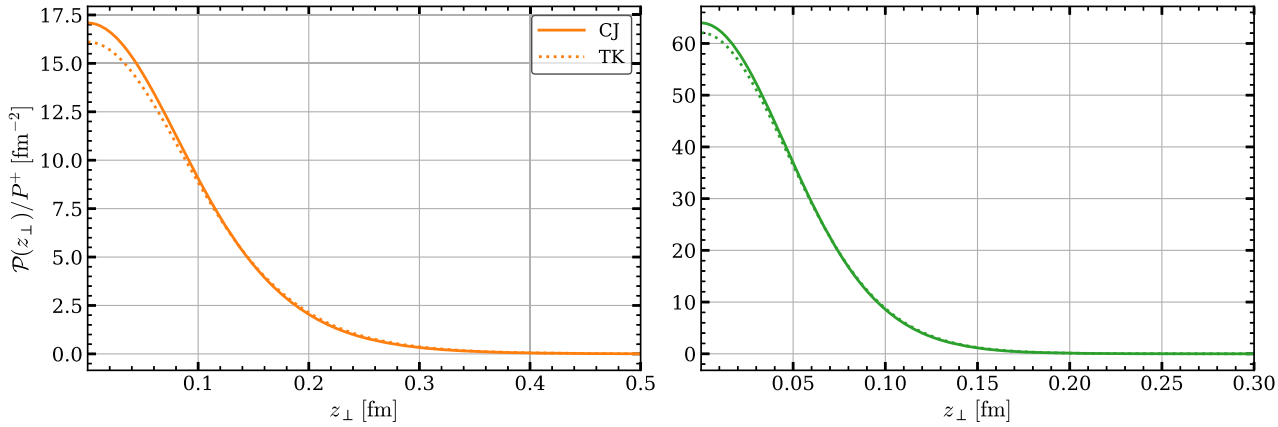


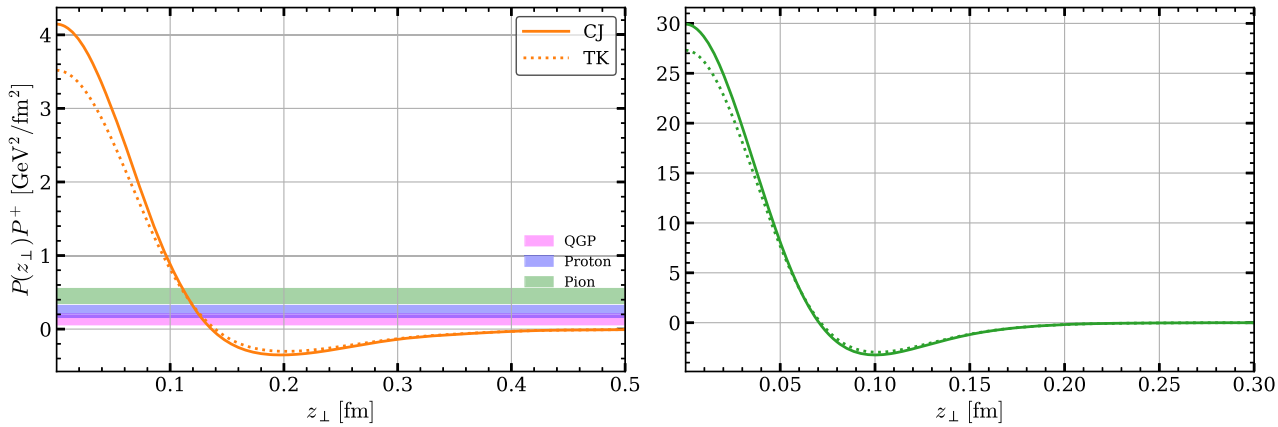
FIG. 4. Variation of all the form factors (GFFs and EMFFs) as a function of momentum transfer is shown for η_c (upper panel) and η_b (lower panel). Note that the normalized D-term, $D(-\vec{\Delta}_\perp^2)/D(-\vec{\Delta}_\perp^2=0)$ is shown for a meaningful comparison.

distribution inside the meson. The mechanical radius is inversely proportional to the value of $D/D(0)$ (see Eq. (D14) of Appendix D). From the Fig. 4, one reckons that the transverse radius associated with η_b is less than η_c, which in turn implies that the force distribution is more concentrated for η_b than η_c. These facts would become clear as we display the mechanical distributions in the transverse plane in the next paragraphs.

In Fig. 5, we show the LF longitudinal momentum distribution (upper panel) and pressure in the transverse plane (lower panel), respectively. The distribution corresponding to the η_c is shown on the left, and that of η_b is shown on the right. For the momentum distribution, we use the normalization factor P^+ so that the normalized distribution $\mathcal{P}/P^+$ integrated over the transverse plane would give one. Note that the momentum distribution is sensitive to the choice of wave function in the region near the center. This is a manifestation of the sensitivity of the A-term to the wave function for large momentum transfer (see Fig. 1). Particularly, we notice that the CJ wave function gives higher momentum density for both the quarkonia. For η_c and η_b, both the wave functions give approximately similar momentum density as the transverse distance increases further from 0.10 fm and 0.05 fm, respectively. We see for the heavier meson η_b, the momentum distribution is more concentrated on the central region than that of η_c. Turning our attention to the pressure inside the mesons, we note that it is obtained by taking appropriate spatial derivatives of the Fourier transform of the D-term [Eq. (20)]. Therefore, the pressure inside the meson is determined by the variation of the $\tilde{D}$ with the transverse distance. In the transverse plane, we observe a node at a finite distance for each meson, where the pressure turns from positive (i.e., attractive) to negative (i.e., repulsive), and finally vanishes as one moves toward the periphery. This effect is a result of the von Laue stability condition [3], which states that $\int dz_\perp z_\perp p(z_\perp) = 0$ (see Eq. (D10) of Appendix D for derivation). We have numerically verified the validity of the von Laue stability condition for different transverse distances, thereby ensuring the consistency of the numerical analysis. Although pressure in general is observed to depend on the chosen wave function type, at least in the central region, the position of the nodes is seen to be mostly independent. The nodes in the η_c and η_b mesons are located approximately at 0.14 fm and 0.07 fm, respectively. To facilitate a direct comparison of numerical magnitudes, we also include pressure bands corresponding to the QGP, proton, and pion obtained in Refs. [1,47,51,55,118], alongside the pressure distributions of the quarkonia. For a thermalized system pressure depends on both the temperature and chemical potential. For the QGP, the band is derived from the thermodynamic pressure calculated using lattice QCD simulations [118] for temperatures in the range $T \approx 0.200$–0.240 GeV at vanishing baryon chemical potential, $\mu_B = 0$. For the proton, we display the pressure



(a) (Color online) Light-front longitudinal momentum density of the mesons η_c (left) and η_b (right).

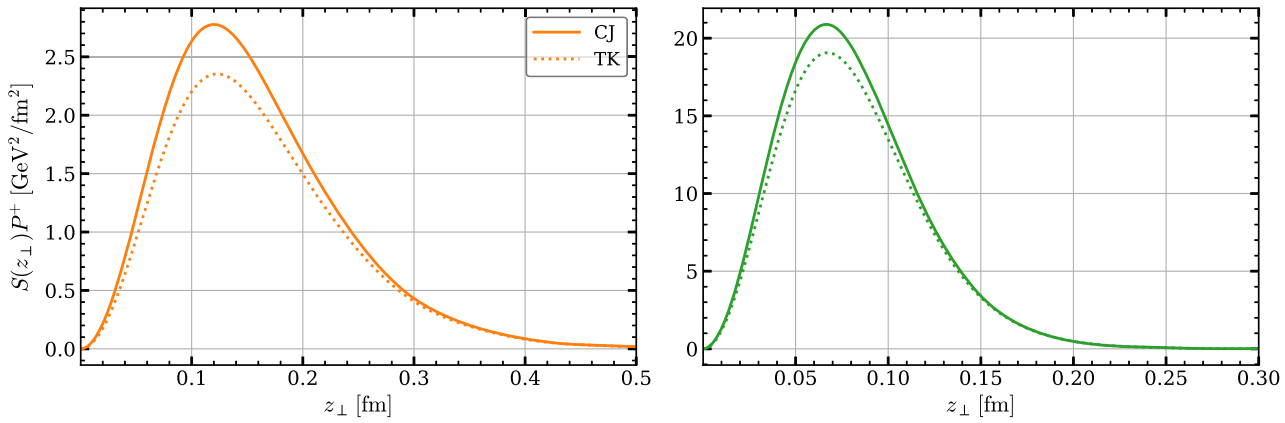


(b) (Color online) The pressure distribution in the transverse plane for the mesons η_c (left) and η_b (right). Also shown are the pressure range of the quark–gluon plasma (QGP) from lattice QCD simulations [116], the peak pressure (with uncertainty) in the proton extracted from experimental measurements [1], and the range of peak pressure values in the pion obtained in various theoretical studies [47, 51, 55].

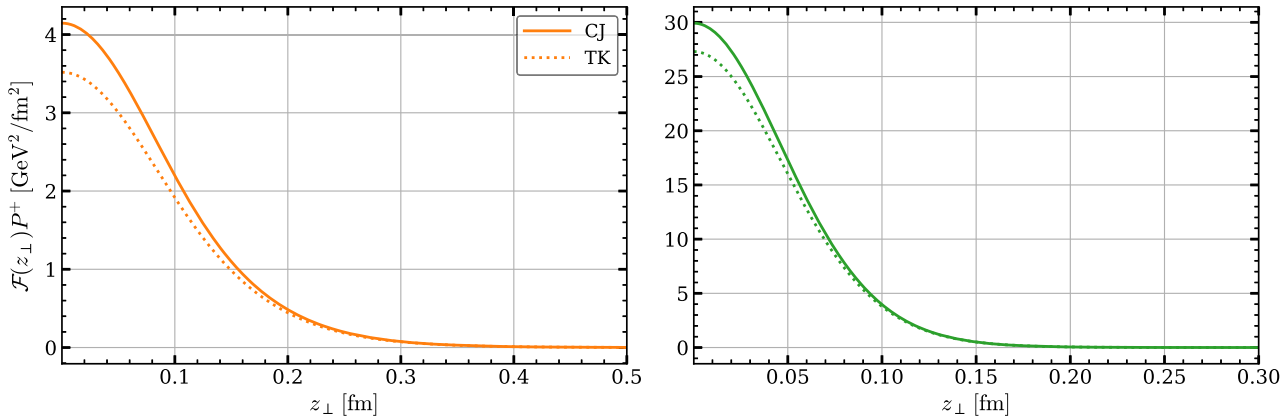
FIG. 5. Dependence of spatial distributions of mechanical properties (momentum and pressure) of mesons on their wave functions.

at $r = 0.25$ fm together with its associated uncertainty, motivated by Ref. [1], where $r^2P(r)$ reaches its maximum near this radius. The pion band is constructed from the peak pressure values reported in Refs. [47,51,55]. We observe that the peak pressures of both the quarkonia are substantially larger than the corresponding values for the QGP, proton, and pion.

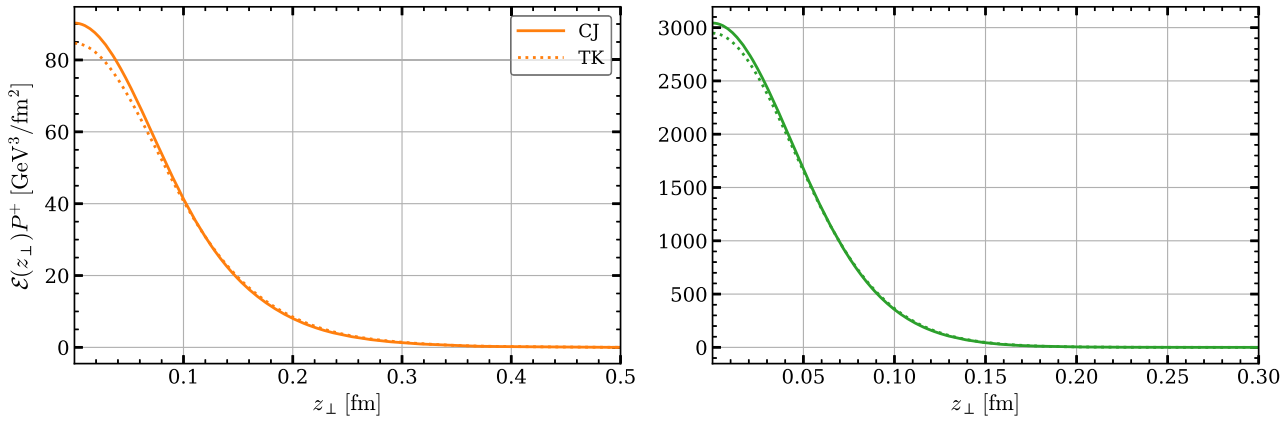
We analyze the shear function, force density, and internal energy density inside the quarkonia in Fig. 6 in the upper, middle, and lower panels, respectively. The distribution of the shear function shows a spike around the point where we observe the nodes in the pressure distribution. Interestingly, in the shear function, we see sensitivity to the wave function at intermediate distances, whereas at the center and periphery, the shear functions for the two sets of wave functions merge. Apart from the von Laue condition, which provides a global condition of stability, one can have the local stability condition, which states that force density should point radially outward, i.e., $\mathscr{F} \equiv p + \frac{1}{2}s > 0$, as postulated in Ref. [111]. As a local stability condition, it provides a stronger stability criterion. The force density displayed in the middle panel of Fig. 6 verifies this local stability criterion for both the mesons, irrespective of the choice of the wave functions. The internal energy density of the quarkonia, as defined in Eq. (24), contains the Fourier transformation of both the GFFs in its expression. As pointed out in Ref. [71], this internal energy density includes kinetic energy of the constituents (including rest mass energies) relative to the center-of-momentum, and the potential energy. We observe that this internal energy is positive for both the quarkonia and decreases with distance from the center. For η_b, we notice that the energy density is very large at the center, which drops rapidly when one approaches the surface of the quarkonium. We also observe that the energy density is sensitive to the choice of the wave function in the central region.



(a) (Color online) Distribution of shear stresses in the transverse plane for the mesons η_c (left) and η_b (right).



(b) (Color online) Force density in the transverse plane for the mesons η_c (left) and η_b (right).



(c) (Color online) Internal energy distribution in the transverse plane for the mesons η_c (left) and η_b (right).

FIG. 6. The wave function dependence of the mechanical distributions (shear, force, and energy) inside η_c and η_b.

We close the discussion by giving several useful length scales that define the spread of the mechanical properties of the quarkonia in the transverse plane. One can then compare it with the length associated with the EMFF, which decides the spread in the charge distribution. A useful quantity is the slope of the corresponding form factors at zero momentum transfer, from which one defines the length scale [55]

$$\langle r^2_{\mathscr{F}} \rangle = -\frac{6}{\mathscr{F}(0)} \frac{d\mathscr{F}}{d\vec{\Delta}^2_\perp}, \tag{28}$$

TABLE I. Mean radii (measured in fm) corresponding to the three form factors and two transverse-plane distributions.

LFWFs	Meson	$\sqrt{\langle r_A^2\rangle}$	$\sqrt{\langle r_D^2\rangle}$	$\sqrt{\langle r_F^2\rangle}$	$\sqrt{\langle z_\perp^2\rangle_{\mathcal{P}}}$	$\sqrt{\langle z_\perp^2\rangle_{\mathscr{F}}}$
CJ	η_c	0.188	0.217	0.202	0.152	0.152
	η_b	0.092	0.076	0.095	0.075	0.075
TK	η_c	0.193	0.237	0.207	0.156	0.155
	η_b	0.093	0.074	0.096	0.076	0.076

where $\mathscr{F}$ can be the GFFs or the EMFFs. The generic radius associated with the A and F-terms is the length associated with the mass and charge distributions. Similarly, we also provide the length associated with the D-term by finding the slope at zero momentum transfer as provided in Ref. [55] for pions. As described in Appendix D, the radii obtained with Eq. (28) correspond to the length scale associated with 3D distributions. Similarly, $2D$ mean radii associated with the momentum and force distribution in the transverse plane are defined in Sec. II C in Eqs. (25) and (26). We provide a comparison of these radii for different choices of wave functions in the Table I. We should mention that the $2D$ and $3D$ radius associated with the A-term are related by $\sqrt{\langle r_A^2\rangle} = \sqrt{\frac{3}{2}}\sqrt{\langle z_\perp^2\rangle_{\mathcal{P}}}$ (see Eq. (D15) of Appendix D). One can see that this equality holds to a good extent in our numerical evaluation of the radius parameters provided in Table I. Moreover, we see that similar to the pion case reported in Refs. [55,119] for charmoinium, the ranking $\sqrt{\langle r^2_{A_{\eta_c}}\rangle} < \sqrt{\langle r^2_{F_{\eta_c}}\rangle} < \sqrt{\langle r^2_{D_{\eta_c}}\rangle}$ hold. However, for the heavier meson, the bottomonium, it no longer holds. In the $2D$ plane, we notice that the momentum and force are distributed almost equally with $\sqrt{\langle z_\perp^2\rangle_{\mathcal{P}}} \approx \sqrt{\langle z_\perp^2\rangle_{\mathscr{F}}}$ for both the quarkonia. The mechanical properties for the bottomonium are spread in a region which is almost half of that of the charmonium, i.e., $\sqrt{\langle z_\perp^2\rangle_{\eta_b}} \approx \frac{1}{2}\sqrt{\langle z_\perp^2\rangle_{\eta_c}}$.

IV. SUMMARY

To summarize the work, we have investigated the mechanical properties and internal force distributions of the heavy pseudoscalar mesons by solving the EMTs within the self-consistent LFQM. This study provides insight into the spatial distributions of energy, pressure, and shear forces inside heavy quarkonia by extracting the gravitational form factors associated with the EMT. In order to properly account for the zero-mode contributions that arise in the light-front dynamics, we adopted the BT construction method following the Ref. [55]. This implementation of the BT framework ensures the restoration of covariance and consistency between different current components for meson systems composed of equal-mass quark and antiquark.

By evaluating the matrix elements of the EMT ($\hat{T}^{\mu\nu}$) using the appropriate mesonic Fock-state expansion and quark-field operators, we derived the A- and D-term GFFs, which primarily encode the internal energy, momentum, pressure, and shear-force distributions inside the meson. The A-term, which is calculated from the good current components of the EMT, is associated with the momentum and mass-energy distribution carried by the constituents, while the D-term characterizes the mechanical properties of the hadron, including the internal pressure and stability conditions. With two distinct light-front wave functions, we have provided a comprehensive description of the mechanical distributions of heavy quarkonia. The A-term is found to satisfy the corresponding sum rule, and the calculated longitudinal momentum density exhibits positive distributions throughout the transverse position space. The pressure distribution, obtained from the D-term, shows positive values in the low-$z_\perp$ region, indicating a strong repulsive force among the constituents, while it becomes negative at larger $z_\perp$, suggesting the presence of an attractive force among the constituents. The stress distribution is found to exhibits the positive distribution all over the $z_\perp$. Similarly, the force density and internal energy density are also found to exhibit positive distributions throughout the transverse plane. In the case of heavy bottomonium, the D-term is found to be of smaller magnitude than the charmonium case. The longitudinal momentum density, internal energy density, pressure, force density, and shear distributions for the bottomonium are found to be larger in magnitude in the central region than those of charmonium in both model wave functions. The mechanical and momentum radii of quarkonia are found to be the same, which are less than their charge radii. All the distributions in this paper are calculated using the 2D Fourier transformation rather than choosing the 3D transformations to avoid the quantum delocalization effects.

Overall, this study provides a comprehensive description of the internal mechanical distributions of heavy quarkonium systems within the framework of light-front dynamics with two distinct light-front wave functions. These findings may serve as useful theoretical inputs for future investigations of gravitational form factors, generalized parton distributions, and lattice QCD studies of heavy hadronic systems. The present work can also be extended to excited states, higher Fock sectors, and spin-dependent mechanical properties in future studies.

ACKNOWLEDGMENTS

This work was partially supported by the Ministry of Education (MoE), Government of India (A. D.), and by the Board of Research in Nuclear Sciences (BRNS) and the Department of Atomic Energy (DAE), Government of India, under Grant No. 57/14/01/2024-BRNS/313 (S. G.). A. D. thanks the YITP International School 2026 (No. YITP-W-25-16), "International School on EIC Physics at Kyoto," where discussions contributed to this work. He acknowledges

financial support from the MoE through the International Conference Visit Scheme of IIT Bhilai for his visit to Japan. He also thanks the organizers of the YITP School for their hospitality in Kyoto, and Prof. Chiho Nonaka and Dr. Cho Win Aung for hosting his research visit at Hiroshima University. S. P. thanks Prof. Oleg V. Teryaev for helpful discussions during his visit to BLTP-JINR, Dubna, Russia, and acknowledges the hospitality of IIT Bhilai and BLTP-JINR, where part of this work was carried out.

DATA AVAILABILITY

There are no publicly available research data or software supporting this manuscript. Requests for further information or data should be sent to the authors.

APPENDIX A: LIGHT-FRONT SPINORS AND LIGHT FRONT SPIN WAVE FUNCTIONS OF PSEUDOSCALAR MESONS

We follow the Lepage-Brodsky (LB) convention [74,120] in our analysis. The LF position coordinates $z_{\rm LF} \equiv z = (z^+, z^1, z^2, z^-)$ and the instant from coordinates $x = (x^0, x^1, x^2, x^3)$ are related by $z^+ = x^0 + x^3$, $z^1 = x^1$, $z^2 = x^2$ and $z^- = x^0 - x^3$. This transformation leads to a nondiagonal metric

$$g_{\mu\nu} = \begin{pmatrix} 0 & 0 & 0 & \frac{1}{2} \\ 0 & -1 & 0 & 0 \\ 0 & 0 & -1 & 0 \\ \frac{1}{2} & 0 & 0 & 0 \end{pmatrix}, \quad g^{\mu\nu} = \begin{pmatrix} 0 & 0 & 0 & 2 \\ 0 & -1 & 0 & 0 \\ 0 & 0 & -1 & 0 \\ 2 & 0 & 0 & 0 \end{pmatrix}. \tag{A1}$$

The inner product between two vectors is defined with the help of the metric as $A \cdot B \equiv g_{\mu\nu} A^\mu B^\nu = \frac{1}{2}(A^+ B^- + A^- B^+) - \vec{A}_\perp \cdot \vec{B}_\perp$. We use the Dirac matrices in the Dirac representation, i.e.,

$$\gamma^0 \equiv \boldsymbol{\beta} = \begin{pmatrix} I & 0 \\ 0 & -I \end{pmatrix}, \qquad \gamma^k = \begin{pmatrix} 0 & \sigma^k \\ -\sigma^k & 0 \end{pmatrix},$$
$$\gamma^5 = \begin{pmatrix} 0 & I \\ I & 0 \end{pmatrix}, \qquad \alpha^k \equiv \boldsymbol{\beta}\gamma^k = \begin{pmatrix} 0 & \sigma^k \\ \sigma^k & 0 \end{pmatrix}, \tag{A2}$$

where I and σ^k are the two dimensional identity and Pauli matrices. The LF Dirac matrices $\gamma^\pm$ are defined as $\gamma^0 \pm \gamma^3$. The LF Dirac spinors are defined as

$$u_{\lambda_q = \pm 1}(p_q) = \frac{1}{\sqrt{p_q^+}} (p_q^+ + \boldsymbol{\beta} m_q + \vec{\alpha}_\perp \cdot \vec{p}_{q\perp}) \chi_\pm, \tag{A3}$$

$$v_{\lambda_{\bar{q}} = \pm 1}(p_{\bar{q}}) = \frac{1}{\sqrt{p_{\bar{q}}^+}} (p_{\bar{q}}^+ - \boldsymbol{\beta} m_{\bar{q}} + \vec{\alpha}_\perp \cdot \vec{p}_{\bar{q}\perp}) \chi_\mp, \tag{A4}$$

where $\chi_+^T = 1/\sqrt{2}(1010)$ and $\chi_-^T = 1/\sqrt{2}(0\,1\,0\,-1)$. Upon simplification, we can get the following four Dirac spinors:

$$u_{\lambda_q = +1}(p_q) = \frac{1}{\sqrt{2p_q^+}} \begin{pmatrix} p_q^+ + m_q \\ p_q^R \\ p_q^+ - m_q \\ p_q^R \end{pmatrix}, \tag{A5}$$

$$u_{\lambda_q = -1}(p_q) = \frac{1}{\sqrt{2p_q^+}} \begin{pmatrix} -p_q^L \\ p_q^+ + m_q \\ p_q^L \\ -(p_q^+ - m_q) \end{pmatrix} \tag{A6}$$

$$v_{\lambda_{\bar{q}} = +1}(p_{\bar{q}}) = \frac{1}{\sqrt{2p_{\bar{q}}^+}} \begin{pmatrix} -p_{\bar{q}}^L \\ p_{\bar{q}}^+ - m_{\bar{q}} \\ p_{\bar{q}}^L \\ -(p_{\bar{q}}^+ + m_{\bar{q}}) \end{pmatrix}, \tag{A7}$$

$$v_{\lambda_{\bar{q}} = -1}(p_{\bar{q}}) = \frac{1}{\sqrt{2p_{\bar{q}}^+}} \begin{pmatrix} p_{\bar{q}}^+ - m_{\bar{q}} \\ p_{\bar{q}}^R \\ p_{\bar{q}}^+ + m_{\bar{q}} \\ p_{\bar{q}}^R \end{pmatrix}, \tag{A8}$$

where we use the notation $p_{q(\bar{q})}^R \equiv p_{q(\bar{q})}^x + i p_{q(\bar{q})}^y$ and $p_{q(\bar{q})}^L \equiv p_{q(\bar{q})}^x - i p_{q(\bar{q})}^y$. For a meson traveling with momenta $\vec{P} = (P^+, \vec{P}_\perp)$, the momentum of the quark and antiquark comprising the valence state of the meson in the LF is expressed as, $\vec{p}_q = (p_q^+ \equiv x_q P^+, \vec{p}_{q\perp} \equiv x_q \vec{P}_\perp + \vec{k}_{q\perp})$ and $\vec{p}_{\bar{q}} = (p_{\bar{q}}^+ \equiv x_{\bar{q}} P^+, \vec{p}_{\bar{q}\perp} \equiv x_{\bar{q}} \vec{P}_\perp + \vec{k}_{\bar{q}\perp})$ such that $\vec{P} = \vec{p}_q + \vec{p}_{\bar{q}}$. The last condition renders the possibility of only two independent variables characterizing the longitudinal and transverse motion, i.e., $x \equiv x_q$ and $\vec{k}_\perp \equiv \vec{k}_{q\perp}$. The antiquark momentum is constrained to be $\vec{p}_{\bar{q}} = (p_{\bar{q}}^+ = (1-x)P^+, \vec{p}_{\bar{q}\perp} = (1-x)\vec{P}_\perp - \vec{k}_\perp)$. One writes the total valence state wave function Ψ as a product of space φ and spin wave functions $\mathcal{S}$, i.e., $\Psi_{\lambda_q \lambda_{\bar{q}}}(x, \vec{k}_\perp) = \varphi(x, \vec{k}_\perp) \mathcal{S}_{\lambda_q \lambda_{\bar{q}}}(x, \vec{k}_\perp)$. The spin wave function of a pseudoscalar meson is obtained by the choice of an appropriate vertex in terms of the quark and antiquark spinors as

$$\mathcal{S}_{\lambda_q \lambda_{\bar{q}}} = \frac{1}{\sqrt{2}} \frac{\bar{u}_{\lambda_q}(p_q) \gamma_5 v_{\lambda_{\bar{q}}}(p_{\bar{q}})}{\sqrt{M_0^2 - (m_q - m_{\bar{q}})^2}},$$
$$\text{where } M_0^2 = \frac{\vec{k}_\perp^2 + m_q^2}{x} + \frac{\vec{k}_\perp^2 + m_{\bar{q}}^2}{1-x}. \tag{A9}$$

Upon explicitly performing the spinor multiplications in Eq. (A9) using Eqs. (A5)–(A8) we get

$$\mathcal{S}_{\lambda_q\lambda_{\bar{q}}} = \frac{1}{\sqrt{2}\sqrt{\vec{k}_\perp^2 + ((1-x)m_q + xm_{\bar{q}})^2}} \times \begin{pmatrix} -k^R & -((1-x)m_q + xm_{\bar{q}}) \\ ((1-x)m_q + xm_{\bar{q}}) & -k^L \end{pmatrix}, \tag{A10}$$

where we label the row (column) starting from $\lambda_{q(\bar{q})} = -1$ to ending at $\lambda_{q(\bar{q})} = 1$. It is worth pointing out that in the spin wave functions given in Eq. (A10) the dependence on the total meson momenta $\vec{P} = (P^+, \vec{P}_\perp)$ cancels out.

APPENDIX B: EVALUATION OF MATRIX ELEMENTS OF EMT OPERATOR

To get the EMT operator, we first write down the free quark fields and their derivatives. The field operators and their derivatives are given by

$$\psi_q(z) = \int \frac{dp_q^+ d^2\vec{p}_q}{2p_q^+(2\pi)^3} \sum_{\lambda_q} u_{\lambda_q}(p_q) b_q(p_q,\lambda_q) e^{-ip_q\cdot z} + \int \frac{dp_{\bar{q}}'^+ d^2\vec{p}'_{\bar{q}}}{2p_{\bar{q}}'^+(2\pi)^3} \sum_{\lambda'_{\bar{q}}} v_{\lambda'_{\bar{q}}}(p'_{\bar{q}}) d^\dagger_{\bar{q}}(p_{\bar{q}'},\lambda'_{\bar{q}}) e^{ip'_{\bar{q}}\cdot z}, \tag{B1}$$

$$\bar{\psi}_q(z) = \int \frac{dp_q'^+ d^2\vec{p}'_q}{2p_q'^+(2\pi)^3} \sum_{\lambda'_q} \bar{u}_{\lambda'_q}(p'_q) b^\dagger_q(p'_q,\lambda'_q) e^{ip'_q\cdot z} + \int \frac{dp_{\bar{q}}^+ d^2\vec{p}_{\bar{q}}}{2p_{\bar{q}}^+(2\pi)^3} \sum_{\lambda_{\bar{q}}} \bar{v}_{\lambda_{\bar{q}}}(p_{\bar{q}}) d_{\bar{q}}(p_{\bar{q}},\lambda_{\bar{q}}) e^{-ip_{\bar{q}}\cdot z}, \tag{B2}$$

$$\partial^\nu\psi_q(z) = -i\int \frac{dp_q^+ d^2\vec{p}_q}{2p_q^+(2\pi)^3} p_q^\nu \sum_{\lambda_q} u_{\lambda_q}(p_q) b_q(p_q,\lambda_q) e^{-ip_q\cdot z} + i\int \frac{dp_{\bar{q}}'^+ d^2\vec{p}'_{\bar{q}}}{2p_{\bar{q}}'^+(2\pi)^3} p_{\bar{q}}'^\nu \sum_{\lambda'_{\bar{q}}} v_{\lambda'_{\bar{q}}}(p'_{\bar{q}}) d^\dagger_{\bar{q}}(p_{\bar{q}'},\lambda'_{\bar{q}}) e^{ip'_{\bar{q}}\cdot z}, \tag{B3}$$

$$\partial^\nu\bar{\psi}_q(z) = i\int \frac{dp_q'^+ d^2\vec{p}'_q}{2p_q'^+(2\pi)^3} p_q'^\nu \sum_{\lambda'_q} \bar{u}_{\lambda'_q}(p'_q) b^\dagger_q(p'_q,\lambda'_q) e^{ip'_q\cdot z} - i\int \frac{dp_{\bar{q}}^+ d^2\vec{p}_{\bar{q}}}{2p_{\bar{q}}^+(2\pi)^3} p_{\bar{q}}^\nu \sum_{\lambda_{\bar{q}}} \bar{v}_{\lambda_{\bar{q}}}(p_{\bar{q}}) d_{\bar{q}}(p_{\bar{q}},\lambda_{\bar{q}}) e^{-ip_{\bar{q}}\cdot z}. \tag{B4}$$

The EMT operator, in terms of the quark field operators, is given by

$$\hat{T}^{\mu\nu} = \frac{1}{4}\bar{\psi}_q(z)(i\gamma^\mu \overleftrightarrow{\partial}^\nu + i\gamma^\nu \overleftrightarrow{\partial}^\mu)\psi_q(z)$$
$$\Rightarrow \hat{T}^{\mu\nu} = \frac{1}{4}\bar{\psi}_q(z)i\gamma^\mu\partial^\nu\psi_q(z) + \frac{1}{4}\bar{\psi}_q(z)i\gamma^\nu\partial^\mu\psi_q(z) - \frac{1}{4}\partial^\nu\bar{\psi}_q(z)i\gamma^\mu\psi_q(z) - \frac{1}{4}\partial^\mu\bar{\psi}_q(z)i\gamma^\nu\psi_q(z),$$

Substituting the quark field operators and their derivative from Eqs. (B1)–(B4) we have

$$\begin{aligned}
\Rightarrow \hat{T}^{\mu\nu} =& \frac{1}{4}\left[\int \frac{dp_q'^+ d^2\vec{p}'_q}{2p_q'^+(2\pi)^3} \sum_{\lambda'_q} \bar{u}_{\lambda'_q}(p'_q) b^\dagger_q(p'_q,\lambda'_q) e^{ip'_q\cdot z} + \int \frac{dp_{\bar{q}}^+ d^2\vec{p}_{\bar{q}}}{2p_{\bar{q}}^+(2\pi)^3} \sum_{\lambda_{\bar{q}}} \bar{v}_{\lambda_{\bar{q}}}(p_{\bar{q}}) d_{\bar{q}}(p_{\bar{q}},\lambda_{\bar{q}}) e^{-ip_{\bar{q}}\cdot z}\right] \\
&\times \left[\int \frac{dp_q^+ d^2\vec{p}_q}{2p_q^+(2\pi)^3} \gamma^\mu p_q^\nu \sum_{\lambda_q} u_{\lambda_q}(p_q) b_q(p_q,\lambda_q) e^{-ip_q\cdot z} - \int \frac{dp_{\bar{q}}'^+ d^2\vec{p}'_{\bar{q}}}{2p_{\bar{q}}'^+(2\pi)^3} \gamma^\mu p_{\bar{q}}'^\nu \sum_{\lambda'_{\bar{q}}} v_{\lambda'_{\bar{q}}}(p'_{\bar{q}}) d^\dagger_{\bar{q}}(p_{\bar{q}'},\lambda'_{\bar{q}}) e^{ip'_{\bar{q}}\cdot z}\right] + (\mu \leftrightarrow \nu) \\
&+ \frac{1}{4}\left[\int \frac{dp_q'^+ d^2\vec{p}'_q}{2p_q'^+(2\pi)^3} \sum_{\lambda'_q} \bar{u}_{\lambda'_q}(p'_q) b^\dagger_q(p'_q,\lambda'_q) e^{ip'_q\cdot z} p_q'^\nu \gamma^\mu - \int \frac{dp_{\bar{q}}^+ d^2\vec{p}_{\bar{q}}}{2p_{\bar{q}}^+(2\pi)^3} \sum_{\lambda_{\bar{q}}} \bar{v}_{\lambda_{\bar{q}}}(p_{\bar{q}}) d_{\bar{q}}(p_{\bar{q}},\lambda_{\bar{q}}) e^{-ip_{\bar{q}}\cdot z} p_{\bar{q}}^\nu \gamma^\mu\right] \\
&\times \left[\int \frac{dp_q^+ d^2\vec{p}_q}{2p_q^+(2\pi)^3} \sum_{\lambda_q} u_{\lambda_q}(p_q) b_q(p_q,\lambda_q) e^{-ip_q\cdot z} + \int \frac{dp_{\bar{q}}'^+ d^2\vec{p}'_{\bar{q}}}{2p_{\bar{q}}'^+(2\pi)^3} \sum_{\lambda'_{\bar{q}}} v_{\lambda'_{\bar{q}}}(p'_{\bar{q}}) d^\dagger_{\bar{q}}(p_{\bar{q}'},\lambda'_{\bar{q}}) e^{ip'_{\bar{q}}\cdot z}\right] + (\mu \leftrightarrow \nu) \\
=& \frac{1}{4}\sum_{\lambda_q,\lambda'_q} \int \frac{dp_q^+ d^2\vec{p}_q}{2p_q^+(2\pi)^3} \frac{dp_q'^+ d^2\vec{p}'_q}{2p_q'^+(2\pi)^3} \bar{u}_{\lambda'_q}(p'_q)[\gamma^\mu(p_q^\nu + p_q'^\nu) + \gamma^\nu(p_q^\mu + p_q'^\mu)] u_{\lambda_q}(p_q) b^\dagger_q(p'_q,\lambda'_q) b_q(p_q,\lambda_q) e^{-i(p_q - p'_q)\cdot z} \\
&- \frac{1}{4}\sum_{\lambda_{\bar{q}},\lambda'_{\bar{q}}} \int \frac{dp_{\bar{q}}^+ d^2\vec{p}_{\bar{q}}}{2p_{\bar{q}}^+(2\pi)^3} \frac{dp_{\bar{q}}'^+ d^2\vec{p}'_{\bar{q}}}{2p_{\bar{q}}'^+(2\pi)^3} \bar{v}_{\lambda_{\bar{q}}}(p_{\bar{q}})[\gamma^\mu(p_{\bar{q}}^\nu + p_{\bar{q}}'^\nu) + \gamma^\nu(p_{\bar{q}}^\mu + p_{\bar{q}}'^\mu)] v_{\lambda'_{\bar{q}}}(p'_{\bar{q}}) d_{\bar{q}}(p_{\bar{q}},\lambda_{\bar{q}}) d^\dagger_{\bar{q}}(p'_{\bar{q}},\lambda'_{\bar{q}}) e^{-i(p_{\bar{q}} - p'_{\bar{q}})\cdot z}.
\end{aligned} \tag{B5}$$

In the above expression, we ignore terms that do not contribute to the matrix elements. We reexpress Eq. (B5) by normal ordering the 2nd term,

$$\Rightarrow \hat{T}^{\mu\nu} = \frac{1}{4}\sum_{\lambda_q,}\sum_{\lambda'_q}\int \frac{dp_q^+ d^2\vec{p}_q}{2p_q^+(2\pi)^3}\frac{dp_q'^+ d^2\vec{p}'_q}{2p_q'^+(2\pi)^3}\bar{u}_{\lambda'_q}(p'_q)[\gamma^\mu(p_q^\nu + p_q'^\nu)+\gamma^\nu(p_q^\mu + p_q'^\mu)]u_{\lambda_q}(p_q)b_q^\dagger(p'_q,\lambda'_q)b_q(p_q,\lambda_q)e^{-i(p_q-p'_q)\cdot z}$$
$$+\frac{1}{4}\sum_{\lambda_{\bar{q}},}\sum_{\lambda'_{\bar{q}}}\int \frac{dp_{\bar{q}}^+ d^2\vec{p}_{\bar{q}}}{2p_{\bar{q}}^+(2\pi)^3}\frac{dp_{\bar{q}}'^+ d^2\vec{p}'_{\bar{q}}}{2p_{\bar{q}}'^+(2\pi)^3}\bar{v}_{\lambda_{\bar{q}}}(p_{\bar{q}})[\gamma^\mu(p_{\bar{q}}^\nu + p_{\bar{q}}'^\nu)+\gamma^\nu(p_{\bar{q}}^\mu + p_{\bar{q}}'^\mu)]v_{\lambda'_{\bar{q}}}(p'_{\bar{q}})d_{\bar{q}}^\dagger(p'_{\bar{q}},\lambda'_{\bar{q}})d_{\bar{q}}(p_{\bar{q}},\lambda_{\bar{q}})e^{-i(p_{\bar{q}}-p'_{\bar{q}})\cdot z}. \tag{B6}$$

From Eq. (B6) it is clear that in the matrix element the first term would correspond to the quark contribution ($\hat{T}_q^{\mu\nu}$) and the second would correspond to the antiquark contribution ($\hat{T}_{\bar{q}}^{\mu\nu}$). The pseudoscalar quarkonia states in the LFQM are expressed as

$$\langle\mathcal{M}(P')| = \langle 0|\int \frac{dx'd^2\vec{k}'_\perp}{2(2\pi)^3\sqrt{x'(1-x')}}\sum_{\lambda'_1,\lambda'_2}\Psi^*_{\lambda'_1\lambda'_2}d_{\bar{q}}((1-x')P'^+,-\vec{k}'_\perp+(1-x')\vec{P}'_\perp,\lambda'_2)b_q(x'P'^+,\vec{k}'_\perp+x'\vec{P}'_\perp,\lambda'_1) \tag{B7}$$

$$|\mathcal{M}(P)\rangle = \int \frac{dxd^2\vec{k}_\perp}{2(2\pi)^3\sqrt{x(1-x)}}\sum_{\lambda_1,\lambda_2}\Psi_{\lambda_1\lambda_2}b_q^\dagger(xP^+,\vec{k}_\perp+x\vec{P}_\perp,\lambda_1)d_{\bar{q}}^\dagger((1-x)P^+,-\vec{k}_\perp+(1-x)\vec{P}_\perp,\lambda_2)|0\rangle \tag{B8}$$

Using Eqs. (B6)–(B8) we can write down the matrix element as the sum of quark and antiquark contributions

$$\begin{aligned}\langle\hat{T}_q^{\mu\nu}\rangle &= \langle 0|\int \frac{dx'd^2\vec{k}'_\perp}{2(2\pi)^3\sqrt{x'(1-x')}}\sum_{\lambda'_1,\lambda'_2}\Psi^*_{\lambda'_1\lambda'_2}d_{\bar{q}}((1-x')P'^+,-\vec{k}'_\perp+(1-x')\vec{P}'_\perp,\lambda'_2)b_q(x'P'^+,\vec{k}'_\perp+x'\vec{P}'_\perp,\lambda'_1)\\
&\times\frac{1}{4}\sum_{\lambda_q,}\sum_{\lambda'_q}\int\frac{dp_q^+d^2\vec{p}_q}{2p_q^+(2\pi)^3}\frac{dp_q'^+d^2\vec{p}'_q}{2p_q'^+(2\pi)^3}\bar{u}_{\lambda'_q}(p'_q)[\gamma^\mu(p_q^\nu+p_q'^\nu)+\gamma^\nu(p_q^\mu+p_q'^\mu)]u_{\lambda_q}(p_q)b_q^\dagger(p'_q,\lambda'_q)b_q(p_q,\lambda_q)\\
&\times\int\frac{dxd^2\vec{k}_\perp}{2(2\pi)^3\sqrt{x(1-x)}}\sum_{\lambda_1,\lambda_2}\Psi_{\lambda_1\lambda_2}b_q^\dagger(xP^+,\vec{k}_\perp+x\vec{P}_\perp,\lambda_1)d_{\bar{q}}^\dagger((1-x)P^+,-\vec{k}_\perp+(1-x)\vec{P}_\perp,\lambda_2)|0\rangle\\
&=\frac{1}{4}\int\frac{dx'd^2\vec{k}'_\perp dp_q^+d^2\vec{p}_q dp_q'^+d^2\vec{p}'_q dxd^2\vec{k}_\perp}{(2(2\pi)^3)^4\sqrt{x(1-x)}\sqrt{x'(1-x')}p_q^+p_q'^+}\sum_{\{\lambda\}}\Psi^*_{\lambda'_1\lambda'_2}\Psi_{\lambda_1\lambda_2}\bar{u}_{\lambda'_q}(p'_q)[\gamma^\mu(p_q^\nu+p_q'^\nu)+\gamma^\nu(p_q^\mu+p_q'^\mu)]u_{\lambda_q}(p_q)\\
&\times\langle 0|d_{\bar{q}}((1-x')P'^+,-\vec{k}'_\perp+(1-x')\vec{P}'_\perp,\lambda'_2)b_q(x'P'^+,\vec{k}'_\perp+x'\vec{P}'_\perp,\lambda'_1)b_q^\dagger(p'_q,\lambda'_q)b_q(p_q,\lambda_q)\\
&\times b_q^\dagger(xP^+,\vec{k}_\perp+x\vec{P}_\perp,\lambda_1)d_{\bar{q}}^\dagger((1-x)P^+,-\vec{k}_\perp+(1-x)\vec{P}_\perp,\lambda_2)|0\rangle,\end{aligned} \tag{B9}$$

$$\begin{aligned}\langle\hat{T}_{\bar{q}}^{\mu\nu}\rangle &= \langle 0|\int \frac{dx'd^2\vec{k}'_\perp}{2(2\pi)^3\sqrt{x'(1-x')}}\sum_{\lambda'_1,\lambda'_2}\Psi^*_{\lambda'_1\lambda'_2}d_{\bar{q}}((1-x')P'^+,-\vec{k}'_\perp+(1-x')\vec{P}'_\perp,\lambda'_2)b_q(x'P'^+,\vec{k}'_\perp+x'\vec{P}'_\perp,\lambda'_1)\\
&\times\frac{1}{4}\sum_{\lambda_{\bar{q}},\lambda'_{\bar{q}}}\int\frac{dp_{\bar{q}}^+d^2\vec{p}_{\bar{q}}}{2p_{\bar{q}}^+(2\pi)^3}\frac{dp_{\bar{q}}'^+d^2\vec{p}'_{\bar{q}}}{2p_{\bar{q}}'^+(2\pi)^3}\bar{v}_{\lambda_{\bar{q}}}(p_{\bar{q}})[\gamma^\mu(p_{\bar{q}}^\nu+p_{\bar{q}}'^\nu)+\gamma^\nu(p_{\bar{q}}^\mu+p_{\bar{q}}'^\mu)]v_{\lambda'_{\bar{q}}}(p'_{\bar{q}})d_{\bar{q}}^\dagger(p'_{\bar{q}},\lambda'_{\bar{q}})d_{\bar{q}}(p_{\bar{q}},\lambda_{\bar{q}})\\
&\times\int\frac{dxd^2\vec{k}_\perp}{2(2\pi)^3\sqrt{x(1-x)}}\sum_{\lambda_1,}\sum_{\lambda_2}\Psi_{\lambda_1\lambda_2}b_q^\dagger(xP^+,\vec{k}_\perp+x\vec{P}_\perp,\lambda_1)d_{\bar{q}}^\dagger((1-x)P^+,-\vec{k}_\perp+(1-x)\vec{P}_\perp,\lambda_2)|0\rangle\\
&=\frac{1}{4}\int\frac{dx'd^2\vec{k}'_\perp dp_q^+d^2\vec{p}_q dp_q'^+d^2\vec{p}'_q dxd^2\vec{k}_\perp}{(2(2\pi)^3)^4\sqrt{x(1-x)}\sqrt{x'(1-x')}p_{\bar{q}}^+p_{\bar{q}}'^+}\sum_{\{\tilde{\lambda}\}}\Psi^*_{\lambda'_1\lambda'_2}\Psi_{\lambda_1\lambda_2}\bar{v}_{\lambda_{\bar{q}}}(p_{\bar{q}})[\gamma^\mu(p_{\bar{q}}^\nu+p_{\bar{q}}'^\nu)+\gamma^\nu(p_{\bar{q}}^\mu+p_{\bar{q}}'^\mu)]v_{\lambda'_{\bar{q}}}(p'_{\bar{q}})\\
&\times\langle 0|d_{\bar{q}}((1-x')P'^+,-\vec{k}'_\perp+(1-x')\vec{P}'_\perp,\lambda'_2)b_q(x'P'^+,\vec{k}'_\perp+x'\vec{P}'_\perp,\lambda'_1)d_{\bar{q}}^\dagger(p'_{\bar{q}},\lambda'_{\bar{q}})d_{\bar{q}}(p_{\bar{q}},\lambda_{\bar{q}})\\
&\times b_q^\dagger(xP^+,\vec{k}_\perp+x\vec{P}_\perp,\lambda_1)d_{\bar{q}}^\dagger((1-x)P^+,-\vec{k}_\perp+(1-x)\vec{P}_\perp,\lambda_2)|0\rangle.\end{aligned} \tag{B10}$$

For the sum over helicity indices we choose the short hand $\{\lambda\} \equiv (\lambda_1, \lambda_2, \lambda_1', \lambda_2', \lambda_q, \lambda_q')$ for quark contribution and $\{\bar{\lambda}\} = (\lambda_1, \lambda_2, \lambda_1', \lambda_2', \lambda_{\bar{q}}, \lambda_{\bar{q}}')$ for antiquark contribution.

To evaluate the quark contribution to the EMT matrix element, we have to simplify the following vacuum expectation value,

$$\langle 0|d_{\bar{q}}((1-x')P'^{+}, -\vec{k}'_{\perp} + (1-x')\vec{P}'_{\perp}, \lambda_2')b_q(x'P'^{+}, \vec{k}'_{\perp} + x'\vec{P}'_{\perp}, \lambda_1')b_q^{\dagger}(p_q', \lambda_q')b_q(p_q, \lambda_q)$$
$$b_q^{\dagger}(xP^{+}, \vec{k}_{\perp} + x\vec{P}_{\perp}, \lambda_1)d_{\bar{q}}^{\dagger}((1-x)P^{+}, -\vec{k}_{\perp} + (1-x)\vec{P}_{\perp}, \lambda_2)|0\rangle. \tag{B11}$$

This expectation value can be simplified by adhering to the LF commutation relations involving the creation and annihilation operators: $\{b_q(p,\lambda), b_q^{\dagger}(p',\lambda')\} = 2(2\pi)^3 p^{+}\delta(p^{+}-p'^{+})\delta^2(\vec{p}_{\perp}-\vec{p}'_{\perp})\delta_{\lambda\lambda'}$ and $\{d_{\bar{q}}(p,\lambda), d_{\bar{q}}^{\dagger}(p',\lambda')\} = 2(2\pi)^3 p^{+}\delta(p^{+}-p'^{+})\delta^2(\vec{p}_{\perp}-\vec{p}'_{\perp})\delta_{\lambda\lambda'}$ with all other anticommutators being zero. One can now calculate the expectation value using Wick's theorem; nevertheless, we work it out explicitly. Let us evaluate the vacuum expectation value by collectively defining the arguments in the operators as $d_{\bar{q}}((1-x')P'^{+}, -\vec{k}'_{\perp} + (1-x')\vec{P}'_{\perp}, \lambda_2')b_q(x'P'^{+}, \vec{k}'_{\perp} + x'\vec{P}'_{\perp}, \lambda_1')$ $b_q^{\dagger}(p_q', \lambda_q')b_q(p_q, \lambda_q)b_q^{\dagger}(xP^{+}, \vec{k}_{\perp} + x\vec{P}_{\perp}, \lambda_1)d_{\bar{q}}^{\dagger}((1-x)P^{+}, -\vec{k}_{\perp} + (1-x)\vec{P}_{\perp}, \lambda_2) \equiv d_{\bar{q}}(1)b_q(2)b_q^{\dagger}(3)b_q(4)b_q^{\dagger}(5)d_{\bar{q}}^{\dagger}(6)$. The expectation value becomes

$$\begin{aligned}
\langle 0|d_{\bar{q}}(1)b_q(2)b_q^{\dagger}(3)b_q(4)b_q^{\dagger}(5)d_{\bar{q}}^{\dagger}(6)|0\rangle &= \langle 0|d_{\bar{q}}(1)b_q(2)b_q^{\dagger}(3)b_q(4)b_q^{\dagger}(5)d_{\bar{q}}^{\dagger}(6)|0\rangle \\
&= \langle 0|d_{\bar{q}}(1)d_{\bar{q}}^{\dagger}(6)b_q(2)b_q^{\dagger}(3)b_q(4)b_q^{\dagger}(5)|0\rangle \\
&= \langle 0|(\delta(16) - d_{\bar{q}}^{\dagger}(6)d_{\bar{q}}(1))(\delta(23) - b_q^{\dagger}(3)b_q(2))(\delta(45) - b_q^{\dagger}(5)b_q(4))|0\rangle \\
&= \langle 0|(\delta(16) - d_{\bar{q}}^{\dagger}(6)d_{\bar{q}}(1))(\delta(23)\delta(45) - \delta(23)b_q^{\dagger}(5)b_q(4) - \delta(45)b_q^{\dagger}(3)b_q(2) \\
&\quad + b_q^{\dagger}(3)b_q(2)b_q^{\dagger}(5)b_q(4))|0\rangle \\
&= \langle 0|(\delta(16) - d_{\bar{q}}^{\dagger}(6)d_{\bar{q}}(1))(\delta(23)\delta(45) - \delta(23)b_q^{\dagger}(5)b_q(4) - \delta(45)b_q^{\dagger}(3)b_q(2) \\
&\quad + b_q^{\dagger}(3)(\delta(25) - b_q^{\dagger}(5)b_q(2))b_q(4))|0\rangle \\
&= \langle 0|(\delta(16) - d_{\bar{q}}^{\dagger}(6)d_{\bar{q}}(1))(\delta(23)\delta(45) - \delta(23)b_q^{\dagger}(5)b_q(4) - \delta(45)b_q^{\dagger}(3)b_q(2) \\
&\quad + b_q^{\dagger}(3)b_q(4)\delta(25) - b_q^{\dagger}(3)b_q^{\dagger}(5)b_q(2)b_q(4))|0\rangle \\
&= \langle 0|(\delta(16)\delta(23)\delta(45) - \delta(16)\delta(23)b_q^{\dagger}(5)b_q(4) - \delta(16)\delta(45)b_q^{\dagger}(3)b_q(2) \\
&\quad + \delta(16)\delta(25)b_q^{\dagger}(3)b_q(4) - \delta(16)b_q^{\dagger}(3)b_q^{\dagger}(5)b_q(2)b_q(4)) \\
&\quad + (-\delta(23)\delta(45)d_{\bar{q}}^{\dagger}(6)d_{\bar{q}}(1) - \delta(23)d_{\bar{q}}^{\dagger}(6)b_q^{\dagger}(5)d_{\bar{q}}(1)b_q(4) \\
&\quad - \delta(45)d_{\bar{q}}^{\dagger}(6)b_q^{\dagger}(3)d_{\bar{q}}(1)b_q(2) + \delta(25)d_{\bar{q}}^{\dagger}(6)b_q^{\dagger}(3)d_{\bar{q}}(1)b_q(4) \\
&\quad + d_{\bar{q}}^{\dagger}(6)b_q^{\dagger}(3)b_q^{\dagger}(5)d_{\bar{q}}(1)b_q(2)b_q(4))|0\rangle \\
&= \langle 0|\delta(16)\delta(23)\delta(45)|0\rangle \\
&= \delta(16)\delta(23)\delta(45).
\end{aligned} \tag{B12}$$

Substituting it in the Eq. (B11) we have

$$\begin{aligned}
&\langle 0|d_{\bar{q}}((1-x')P'^{+}, -\vec{k}'_{\perp} + (1-x')\vec{P}'_{\perp}, \lambda_2')b_q(x'P'^{+}, \vec{k}'_{\perp} + x'\vec{P}'_{\perp}, \lambda_1')b_q^{\dagger}(p_q', \lambda_q')b_q(p_q, \lambda_q) \\
&\quad \times b_q^{\dagger}(xP^{+}, \vec{k}_{\perp} + x\vec{P}_{\perp}, \lambda_1)d_{\bar{q}}^{\dagger}((1-x)P^{+}, -\vec{k}_{\perp} + (1-x)\vec{P}_{\perp}, \lambda_2)|0\rangle \\
&= (2(2\pi)^3)^3(1-x)P^{+}\delta((1-x')P'^{+} - (1-x)P^{+})\delta^2(-\vec{k}'_{\perp} + (1-x')\vec{P}'_{\perp} + \vec{k}_{\perp} - (1-x)\vec{P}_{\perp})\delta_{\lambda_2\lambda_2'} \\
&\quad \times p_q'^{+}\delta(x'P'^{+} - p_q'^{+})\delta^2(\vec{k}'_{\perp} + x'\vec{P}'_{\perp} - \vec{p}'_{q\perp})\delta_{\lambda_1'\lambda_q'}p_q^{+}\delta(xP^{+} - p_q^{+})\delta^2(\vec{k}_{\perp} + x\vec{P}_{\perp} - \vec{p}_{q\perp})\delta_{\lambda_q\lambda_1}.
\end{aligned} \tag{B13}$$

Integrating over the variables x', $\vec{k}'_{\perp}$, $p_q'^{+}$, $\vec{p}'_{q\perp}$, p_q^{+}, and $\vec{p}_{q\perp}$ and summing over λ_1, λ_1', and λ_2' in Eq. (B9) with the use of Eq. (B13) we have

$$\langle \hat{T}^{\mu\nu}_{q} \rangle = \int \frac{dx\, d^2\vec{k}_\perp}{2(2\pi)^3} \varphi^*(x,\vec{k}'_\perp)\varphi(x,\vec{k}_\perp) \sum_{\lambda_q,\lambda'_q,\lambda_2} \mathcal{S}^*_{\lambda'_q\lambda_2}(x,\vec{k}'_\perp) U^{\mu\nu}_{\lambda'_q\lambda_q} \mathcal{S}_{\lambda_q\lambda_2}(x,\vec{k}_\perp)$$
$$= \int \frac{dx\, d^2\vec{k}_\perp}{2(2\pi)^3} \varphi^*(x,\vec{k}'_\perp)\varphi(x,\vec{k}_\perp) S^{\mu\nu}_{q}, \tag{B14}$$

where the following definitions are used

$$U^{\mu\nu}_{\lambda'_q\lambda_q} \equiv \frac{1}{4x} \bar{u}_{\lambda'_q}(p'_q)[\gamma^\mu p^\nu_{sq} + \gamma^\nu p^\mu_{sq}] u_{\lambda_q}(p_q),$$
$$S^{\mu\nu}_{q} \equiv \sum_{\lambda_q,\lambda'_q,\lambda_2} \mathcal{S}^*_{\lambda'_q\lambda_2}(x,\vec{k}'_\perp) U^{\mu\nu}_{\lambda'_q\lambda_q} \mathcal{S}_{\lambda_q\lambda_2}(x,\vec{k}_\perp),$$
$$p_q = (p^-_q, p^+_q, \vec{p}_{q\perp}) = \left(\frac{\vec{p}^2_{q\perp} + m^2_q}{p^+_q}, xP^+, \vec{k}_\perp \right),$$
$$p'_q = (p'^-_q, p'^+_q, \vec{p}'_{q\perp}) = \left(\frac{\vec{p}'^2_{q\perp} + m^2_q}{p'^+_q}, xP^+, \vec{k}_\perp + \vec{\Delta}_\perp \right),$$
$$p_{sq} = p_q + p'_q$$
$$\vec{k}'_\perp = \vec{k}_\perp + (1-x)\vec{\Delta}_\perp. \tag{B15}$$

For the evaluation of the antiparticle contribution to the matrix element provided in Eq. (B10), we need to evaluate the following vacuum expectation value:

$$\langle 0| d_{\bar{q}}((1-x')P'^+, -\vec{k}'_\perp + (1-x')\vec{P}'_\perp, \lambda'_2) b_q(x'P'^+, \vec{k}'_\perp + x'\vec{P}'_\perp, \lambda'_1) d^\dagger_{\bar{q}}(p'_{\bar{q}}, \lambda'_{\bar{q}}) d_{\bar{q}}(p_{\bar{q}}, \lambda_{\bar{q}})$$
$$b^\dagger_q(xP^+, \vec{k}_\perp + x\vec{P}_\perp, \lambda_1) d^\dagger_{\bar{q}}((1-x)P^+, -\vec{k}_\perp + (1-x)\vec{P}_\perp, \lambda_2)|0\rangle$$
$$\equiv \langle 0| d_{\bar{q}}(1) b_q(2) d^\dagger_{\bar{q}}(3) d_{\bar{q}}(4) b^\dagger_q(5) d^\dagger_{\bar{q}}(6)|0\rangle$$
$$= \langle 0| b_q(2) b^\dagger_q(5) d_{\bar{q}}(1) d^\dagger_{\bar{q}}(3) d_{\bar{q}}(4) d^\dagger_{\bar{q}}(6)|0\rangle$$
$$= \langle 0| : b_q(2) b^\dagger_q(5) d_{\bar{q}}(1) d^\dagger_{\bar{q}}(3) d_{\bar{q}}(4) d^\dagger_{\bar{q}}(6) : + \delta(25)\delta(13)\delta(46)|0\rangle$$
$$= \delta(25)\delta(13)\delta(46)$$
$$= (2(2\pi)^3)^3 xP^+ \delta(x'P'^+ - xP^+) \delta^2(\vec{k}'_\perp + x'\vec{P}'_\perp - \vec{k}_\perp - x\vec{P}_\perp) \delta_{\lambda'_1\lambda_1}$$
$$\times 2p'^+_{\bar{q}} \delta(p'^+_{\bar{q}} - (1-x')P'^+) \delta^2(-\vec{k}'_\perp + (1-x')\vec{P}'_\perp - \vec{p}'_{\bar{q}\perp}) \delta_{\lambda'_2\lambda'_{\bar{q}}}$$
$$\times 2p^+_{\bar{q}} \delta(p^+_{\bar{q}} - (1-x)P^+) \delta^2(-\vec{k}_\perp + (1-x)\vec{P}_\perp - \vec{p}_{\bar{q}\perp}) \delta_{\lambda_{\bar{q}}\lambda_2}. \tag{B16}$$

Integrating over the variables x', $\vec{k}'_\perp$, $p'^+_{\bar{q}}$, $\vec{p}'_{\bar{q}\perp}$, $p^+_{\bar{q}}$, and $\vec{p}_{\bar{q}\perp}$ and summing over λ_2, λ'_1, and λ'_2 in Eq. (B10) with the use of Eq. (B16) we have

$$\langle \hat{T}^{\mu\nu}_{\bar{q}} \rangle = \int \frac{dx\, d^2\vec{k}_\perp}{2(2\pi)^3} \varphi^*(x,\vec{\tilde{k}}_\perp)\varphi(x,\vec{k}_\perp) \sum_{\lambda_{\bar{q}},\lambda'_{\bar{q}},\lambda_1} \mathcal{S}_{\lambda_1\lambda_{\bar{q}}}(x,\vec{k}_\perp) V^{\mu\nu}_{\lambda_{\bar{q}}\lambda'_{\bar{q}}} \mathcal{S}^*_{\lambda_1\lambda'_{\bar{q}}}(x,\vec{\tilde{k}}_\perp)$$
$$= \int \frac{dx\, d^2\vec{k}_\perp}{2(2\pi)^3} \varphi^*(x,\vec{\tilde{k}}_\perp)\varphi(x,\vec{k}_\perp) S^{\mu\nu}_{\bar{q}}, \tag{B17}$$

where we use the following definitions:

$$
\begin{aligned}
V^{\mu\nu}_{\lambda_{\bar{q}}\lambda'_{\bar{q}}} &\equiv \frac{1}{4(1-x)}\,\bar{v}_{\lambda_{\bar{q}}}(p_{\bar{q}})[\gamma^\mu p^\nu_{s\bar{q}} + \gamma^\nu p^\mu_{s\bar{q}}]v_{\lambda'_{\bar{q}}}(p'_{\bar{q}}),\\
S^{\mu\nu}_{\bar{q}} &\equiv \sum_{\lambda_{\bar{q}},\lambda'_{\bar{q}},\lambda_1} \mathcal{S}_{\lambda_1\lambda_{\bar{q}}}(x,\vec{k}_\perp)V^{\mu\nu}_{\lambda_{\bar{q}}\lambda'_{\bar{q}}}\mathcal{S}^*_{\lambda_1\lambda'_{\bar{q}}}(x,\vec{\tilde{k}}_\perp),\\
p_{\bar{q}} &= (p^-_{\bar{q}}, p^+_{\bar{q}}, \vec{p}_{\bar{q}\perp}) = \left(\frac{\vec{p}^{\,2}_{\bar{q}\perp}+m^2_{\bar{q}}}{p^+_{\bar{q}}}, (1-x)P^+, -\vec{k}_\perp\right),\\
p'_q &= (p'^-_{\bar{q}}, p'^+_{\bar{q}}, \vec{p}'_{\bar{q}\perp}) = \left(\frac{\vec{p}'^2_{\bar{q}\perp}+m^2_{\bar{q}}}{p'^+_{\bar{q}}}, (1-x)P^+, -\vec{k}_\perp+\vec{\Delta}_\perp\right),\\
p_{s\bar{q}} &= p_{\bar{q}} + p'_{\bar{q}}\\
\vec{\tilde{k}}_\perp &= \vec{k}_\perp - x\vec{\Delta}_\perp.
\end{aligned}
\tag{B18}
$$

1. Evaluation of the quark contribution

Using Eqs. (B14) and (B15) we write the quark contribution as

$$
\langle \hat{T}^{\mu\nu}_q \rangle = \int \frac{dx d^2\vec{k}_\perp}{2(2\pi)^3}\varphi^*(x,\vec{k}'_\perp)\varphi(x,\vec{k}_\perp)S^{\mu\nu}_q, \qquad S^{\mu\nu}_q = \sum_{\lambda_q,\lambda'_q,\lambda_2}\mathcal{S}^*_{\lambda'_q\lambda_2}(x,\vec{k}'_\perp)U^{\mu\nu}_{\lambda'_q\lambda_q}\mathcal{S}_{\lambda_q\lambda_2}(x,\vec{k}_\perp). \tag{B19}
$$

Apart from space wave functions (which are model dependent), this contribution is directly proportional to the spin trace for the tensor current $S^{\mu\nu}_q$. The spin trace of the tensor current can be performed as follows:

$$
S^{\mu\nu}_q = \mathrm{Tr}[\mathcal{S}\mathcal{S}'^\dagger U^{\mu\nu}], \quad \text{where } \mathcal{S} \text{ are matrices corresponding to spin wave functions.} \tag{B20}
$$

The spin wave function $\mathcal{S}$ is the same as Eq. (A10) whereas the spin wave function $\mathcal{S}' = \mathcal{S}(x,\vec{k}'_\perp = \vec{k}_\perp + (1-x)\vec{\Delta}_\perp)$. The multiplication of the spin wave functions can be obtained as

$$
\begin{aligned}
\mathcal{S}\mathcal{S}'^\dagger &= \mathcal{N}\begin{pmatrix} -k^R & -((1-x)m_q + xm_{\bar{q}}) \\ ((1-x)m_q + xm_{\bar{q}}) & -k^L \end{pmatrix}\begin{pmatrix} -k'^L & ((1-x)m_q + xm_{\bar{q}}) \\ -((1-x)m_q + xm_{\bar{q}}) & -k'^R \end{pmatrix}\\
&= \mathcal{N}\begin{pmatrix} k^R k'^L + ((1-x)m_q + xm_{\bar{q}})^2 & ((1-x)m_q + xm_{\bar{q}})(k'^R - k^R) \\ ((1-x)m_q + xm_{\bar{q}})(k^L - k'^L) & k^L k'^R + ((1-x)m_q + xm_{\bar{q}})^2 \end{pmatrix},
\end{aligned}
\tag{B21}
$$

where the shorthand $\mathcal{N} \equiv 2\sqrt{(\vec{k}^2_\perp + ((1-x)m_q + xm_{\bar{q}})^2)(\vec{k}'^2_\perp + ((1-x)m_q + xm_{\bar{q}})^2)}$. Substituting the results $k^R k'^L = \vec{k}_\perp\cdot\vec{k}'_\perp + i(\vec{k}'_\perp\times\vec{k}_\perp)_z = k^2_\perp + (1-x)\vec{\Delta}\cdot\vec{k}_\perp + i(1-x)(\vec{\Delta}_\perp\times\vec{k}_\perp)_z$, $k'^R - k^R = (1-x)\Delta^R_\perp$, and $k^L - k'^L = -(1-x)\Delta^L_\perp$, the product of spin matrices in Eq. (B21) becomes

$$
\mathcal{S}\mathcal{S}'^\dagger = \mathcal{N}\begin{pmatrix} \vec{k}^2_\perp + (1-x)\vec{\Delta}\cdot\vec{k}_\perp + i(1-x)(\vec{\Delta}_\perp\times\vec{k}_\perp)_z + \tilde{m}^2 & \tilde{m}(1-x)\Delta^R_\perp \\ -\tilde{m}(1-x)\Delta^L_\perp & \vec{k}^2_\perp + (1-x)\vec{\Delta}\cdot\vec{k}_\perp - i(1-x)(\vec{\Delta}_\perp\times\vec{k}_\perp)_z + \tilde{m}^2 \end{pmatrix}, \tag{B22}
$$

where $\tilde{m} = (1-x)m_q + xm_{\bar{q}}$ which becomes equal to the quark masses in a symmetric mass system such as quarkonia, i.e., $\tilde{m} = m_{\bar{q}} = m_q$. For our purpose, we need the explicit evaluation of the components of $U^{\mu\nu}$. Multiplying the appropriate spinors (with the help of the spinor multiplication table provided in Ref. [120]), these components are given by

$$
U^{++}_{\lambda'_q\lambda_q} = \frac{1}{4x}\bar{u}_{\lambda'_q}(p'_q)[\gamma^+ p^+_{sq} + \gamma^+ p^+_{sq}]u_{\lambda_q}(p_q) = P^+\bar{u}_{\lambda'_q}(p'_q)\gamma^+ u_{\lambda_q}(p_q) = 2xP^{+2}I, \tag{B23}
$$

$$U^{+-}_{\lambda'_q\lambda_q} = \frac{1}{4x}\bar{u}_{\lambda'_q}(p'_q)[\gamma^+ p^-_{sq} + \gamma^- p^+_{sq}]u_{\lambda_q}(p_q)$$
$$= \frac{2\vec{k}_\perp^2 + \vec{\Delta}_\perp^2 + 2\vec{k}_\perp\cdot\vec{\Delta}_\perp + 2m_q^2}{2x} I + \frac{1}{x}\begin{pmatrix} \vec{k}_\perp^2 + \vec{k}_\perp\cdot\vec{\Delta}_\perp + m_q^2 - i(\vec{\Delta}_\perp\times\vec{k}_\perp)_z & -m_q\Delta_\perp^R \\ m_q\Delta_\perp^L & \vec{k}_\perp^2 + \vec{k}_\perp\cdot\vec{\Delta}_\perp + m_q^2 + i(\vec{\Delta}_\perp\times\vec{k}_\perp)_z \end{pmatrix}$$
$$= \frac{4\vec{k}_\perp^2 + \vec{\Delta}_\perp^2 + 4\vec{k}_\perp\cdot\vec{\Delta}_\perp + 4m_q^2}{2x} I + \frac{1}{x}\begin{pmatrix} -i(\vec{\Delta}_\perp\times\vec{k}_\perp)_z & -m_q\Delta_\perp^R \\ m_q\Delta_\perp^L & +i(\vec{\Delta}_\perp\times\vec{k}_\perp)_z \end{pmatrix} \tag{B24}$$

$$U^{+i}_{\lambda'_q\lambda_q} = \frac{1}{4x}\bar{u}_{\lambda'_q}(p'_q)[\gamma^+ p^i_{sq} + \gamma^i p^+_{sq}]u_{\lambda_q}(p_q) = \frac{P^+}{2}(2k^i_\perp + \Delta^i_\perp)I + \frac{P^+}{2}\begin{pmatrix} 2k^i_\perp + \Delta^i_\perp + i\epsilon^{ij}\Delta^j_\perp & 0 \\ 0 & 2k^i_\perp + \Delta^i_\perp - i\epsilon^{ij}\Delta^j_\perp \end{pmatrix}$$
$$= P^+(2k^i_\perp + \Delta^i_\perp)I + \frac{P^+}{2}\begin{pmatrix} +i\epsilon^{ij}\Delta^j_\perp & 0 \\ 0 & -i\epsilon^{ij}\Delta^j_\perp \end{pmatrix}, \tag{B25}$$

$$U^{ij}_{\lambda'_q\lambda_q} = \frac{1}{4x}\bar{u}_{\lambda'_q}(p'_q)[\gamma^i p^j_{sq} + \gamma^j p^i_{sq}]u_{\lambda_q}(p_q)$$
$$= \frac{1}{4x}\left[p^j_{sq}\begin{pmatrix} 2k^i_\perp + \Delta^i_\perp + i\epsilon^{ik}\Delta^k_\perp & 0 \\ 0 & 2k^i_\perp + \Delta^i_\perp - i\epsilon^{ik}\Delta^k_\perp \end{pmatrix} + p^i_{sq}\begin{pmatrix} 2k^j_\perp + \Delta^j_\perp + i\epsilon^{jk}\Delta^k_\perp & 0 \\ 0 & 2k^j_\perp + \Delta^j_\perp - i\epsilon^{jk}\Delta^k_\perp \end{pmatrix}\right]$$
$$= \frac{1}{4x}\left[2(2k^i_\perp + \Delta^i_\perp)(2k^j_\perp + \Delta^j_\perp)I + p^j_{sq}\begin{pmatrix} i\epsilon^{ik}\Delta^k_\perp & 0 \\ 0 & -i\epsilon^{ik}\Delta^k_\perp \end{pmatrix} + p^i_{sq}\begin{pmatrix} i\epsilon^{jk}\Delta^k_\perp & 0 \\ 0 & -i\epsilon^{jk}\Delta^k_\perp \end{pmatrix}\right], \tag{B26}$$

$$U^{-i}_{\lambda'_q\lambda_q} = \frac{1}{4x}\bar{u}_{\lambda'_q}(p'_q)[\gamma^- p^i_{sq} + \gamma^i p^-_{sq}]u_{\lambda_q}(p_q)$$
$$= \frac{1}{4x}\left[\frac{2p^i_{sq}}{xP^+}\begin{pmatrix} \vec{k}_\perp^2 + \vec{k}_\perp\cdot\vec{\Delta}_\perp + m_q^2 - i(\vec{\Delta}_\perp\times\vec{k}_\perp)_z & -m_q\Delta_\perp^R \\ m_q\Delta_\perp^L & \vec{k}_\perp^2 + \vec{k}_\perp\cdot\vec{\Delta}_\perp + m_q^2 + i(\vec{\Delta}_\perp\times\vec{k}_\perp)_z \end{pmatrix}\right.$$
$$\left. + p^-_{sq}\begin{pmatrix} 2k^i_\perp + \Delta^i_\perp + i\epsilon^{ik}\Delta^k_\perp & 0 \\ 0 & 2k^i_\perp + \Delta^i_\perp - i\epsilon^{ik}\Delta^k_\perp \end{pmatrix}\right]$$
$$= \frac{1}{4x}\left[\frac{2k^i_\perp + \Delta^i_\perp}{xP^+}(4\vec{k}_\perp^2 + \vec{\Delta}_\perp^2 + 4\vec{k}_\perp\cdot\vec{\Delta}_\perp + 4m_q^2)I + \frac{2(2k^i_\perp + \Delta^i_\perp)}{xP^+}\begin{pmatrix} -i(\vec{\Delta}_\perp\times\vec{k}_\perp)_z & -m_q\Delta_\perp^R \\ m_q\Delta_\perp^L & +i(\vec{\Delta}_\perp\times\vec{k}_\perp)_z \end{pmatrix}\right.$$
$$\left. + p^-_{sq}\begin{pmatrix} +i\epsilon^{ik}\Delta^k_\perp & 0 \\ 0 & -i\epsilon^{ik}\Delta^k_\perp \end{pmatrix}\right], \tag{B27}$$

$$U^{--}_{\lambda'_q\lambda_q} = \frac{1}{4x}\bar{u}_{\lambda'_q}(p'_q)[\gamma^- p^-_{sq} + \gamma^- p^-_{sq}]u_{\lambda_q}(p_q)$$
$$= \frac{p^-_{sq}}{x^2P^+}\begin{pmatrix} \vec{k}_\perp^2 + \vec{k}_\perp\cdot\vec{\Delta}_\perp + m_q^2 - i(\vec{\Delta}_\perp\times\vec{k}_\perp)_z & -m_q\Delta_\perp^R \\ m_q\Delta_\perp^L & \vec{k}_\perp^2 + \vec{k}_\perp\cdot\vec{\Delta}_\perp + m_q^2 + i(\vec{\Delta}_\perp\times\vec{k}_\perp)_z \end{pmatrix}$$
$$= \frac{(2\vec{k}_\perp^2 + \vec{\Delta}_\perp^2 + 2\vec{k}_\perp\cdot\vec{\Delta}_\perp + 2m_q^2)(\vec{k}_\perp^2 + \vec{k}_\perp\cdot\vec{\Delta}_\perp + m_q^2)}{x^3(P^+)^2} I + \frac{2\vec{k}_\perp^2 + \vec{\Delta}_\perp^2 + 2\vec{k}_\perp\cdot\vec{\Delta}_\perp + 2m_q^2}{x^3(P^+)^2}$$
$$\times\begin{pmatrix} -i(\vec{\Delta}_\perp\times\vec{k}_\perp)_z & -m_q\Delta_\perp^R \\ m_q\Delta_\perp^L & +i(\vec{\Delta}_\perp\times\vec{k}_\perp)_z \end{pmatrix}. \tag{B28}$$

The "I" in the above result is the identity matrix and ϵ^{ij} is the antisymmetric tensor. These forms of $U^{\mu\nu}$ are particularly useful in calculating the spin trace of the tensor current $S_q^{\mu\nu}$. Substituting the results of (B23)–(B28) in Eq. (B20), different components of $S_q^{\mu\nu}$ are obtained and provided in the Table II.

TABLE II. The spin traces for the tensor current $S_q^{\mu\nu} = \mathrm{Tr}[\mathcal{S}\mathcal{S}'^{\dagger}U^{\mu\nu}]$ is given below for easy reference. We use the following definition $\underline{k}_\perp^2 \equiv \vec{k}_\perp^2 + \vec{k}_\perp \cdot \vec{\Delta}_\perp + m_q^2$.

$(\mu\nu)$	$S_q^{\mu\nu}$
$(++)$	$\frac{2x(P^+)^2(\vec{k}_\perp\cdot\vec{k}'_\perp+m_q^2)}{\sqrt{\vec{k}_\perp^2+m_q^2}\sqrt{\vec{k}'^2_\perp+m_q^2}}$
$(+-)$	$\frac{2(\vec{k}_\perp\cdot\vec{k}'_\perp+m_q^2)(\underline{k}_\perp^2+\frac{\vec{\Delta}_\perp^2}{4})+m_q^2(1-x)\vec{\Delta}_\perp^2+(1-x)(\vec{\Delta}_\perp\times\vec{k}_\perp)_z^2}{x\sqrt{\vec{k}_\perp^2+m_q^2}\sqrt{\vec{k}'^2_\perp+m_q^2}}$
$(+i)$	$\frac{P^+(2k_\perp^i+\Delta_\perp^i)(\vec{k}_\perp\cdot\vec{k}'_\perp+m_q^2)}{\sqrt{\vec{k}_\perp^2+m_q^2}\sqrt{\vec{k}'^2_\perp+m_q^2}} - \frac{P^+\epsilon^{ij}\Delta_\perp^j(1-x)(\vec{\Delta}_\perp\times\vec{k}_\perp)_z}{2\sqrt{\vec{k}_\perp^2+m_q^2}\sqrt{\vec{k}'^2_\perp+m_q^2}}$
(ij)	$\frac{(\vec{k}_\perp\cdot\vec{k}'_\perp+m_q^2)(2k_\perp^i+\Delta_\perp^i)(2k_\perp^j+\Delta_\perp^j)}{2x\sqrt{\vec{k}_\perp^2+m_q^2}\sqrt{\vec{k}'^2_\perp+m_q^2}} - \frac{(1-x)(\vec{\Delta}_\perp\times\vec{k}_\perp)_z\Delta_\perp^k(\epsilon^{ik}(2k_\perp^j+\Delta_\perp^j)+\epsilon^{jk}(2k_\perp^i+\Delta_\perp^i))}{4x\sqrt{\vec{k}_\perp^2+m_q^2}\sqrt{\vec{k}'^2_\perp+m_q^2}}$
$(-i)$	$\frac{(2k_\perp^i+\Delta_\perp^i)(m_q^2(1-x)\vec{\Delta}_\perp^2+(\vec{k}_\perp\cdot\vec{k}'_\perp+m_q^2)(2\underline{k}_\perp^2+\frac{\vec{\Delta}_\perp^2}{2})+(1-x)(\vec{\Delta}_\perp\times\vec{k}_\perp)_z^2)}{2x^2P^+\sqrt{\vec{k}_\perp^2+m_q^2}\sqrt{\vec{k}'^2_\perp+m_q^2}} - \frac{(2\underline{k}_\perp^2+\vec{\Delta}_\perp^2)(1-x)(\vec{\Delta}_\perp\times\vec{k}_\perp)_z\epsilon^{ik}\Delta_\perp^k}{4x^2P^+\sqrt{\vec{k}_\perp^2+m_q^2}\sqrt{\vec{k}'^2_\perp+m_q^2}}$
$(--)$	$\frac{(2\underline{k}_\perp^2+\vec{\Delta}_\perp^2)(2m_q^2(1-x)\vec{\Delta}_\perp^2+2(1-x)(\vec{\Delta}_\perp\times\vec{k}_\perp)_z^2+2\underline{k}_\perp^2(\vec{k}_\perp\cdot\vec{k}'_\perp+m_q^2))}{2x^3(P^+)^2\sqrt{\vec{k}_\perp^2+m_q^2}\sqrt{\vec{k}'^2_\perp+m_q^2}}$

2. Connecting the antiquark contribution to the quark contribution

In this section, we connect the antiquark contribution to the matrix element of the EMT operator provided in Eqs. (B16) and (B17) to the quark contribution provided in Eqs. (B14) and (B15). Even though we are only dealing with a symmetric mass system (quarkonia), we keep the discussion more general. To see the connection, we write the integral in Eq. (B14) in terms of the transformed variables, $x \to (1-x)$ and $\vec{k}_\perp \to -\vec{k}_\perp$ and with a real replacement $m_q \leftrightarrow m_{\bar{q}}$. The replacement of the mass only matters when $m_q \neq m_{\bar{q}}$. Under these transformations, the space wave function transforms as, $\varphi(-\vec{k}_\perp, 1-x, m_{\bar{q}}, m_q) = \varphi(\vec{k}_\perp, x, m_q, m_{\bar{q}})$. Similarly, the spin trace part $S_q^{\mu\nu}$, will undergo a change. The transformed spin matrices $\mathcal{S} \to \tilde{\mathcal{S}}$ and $\mathcal{S}'^{\dagger} \to \tilde{\mathcal{S}}'^{\dagger}$ are

$$\mathcal{S} = \frac{1}{\sqrt{2}\sqrt{\vec{k}_\perp^2+\tilde{m}^2}}\begin{pmatrix} -k^R & -\tilde{m} \\ \tilde{m} & -k^L \end{pmatrix} \to \tilde{\mathcal{S}} = \frac{1}{\sqrt{2}} \times \frac{1}{\sqrt{\vec{k}_\perp^2+\tilde{m}^2}}\begin{pmatrix} k^R & -\tilde{m} \\ \tilde{m} & k^L \end{pmatrix}, \qquad \tilde{\mathcal{S}}'^{\dagger} = \frac{1}{\sqrt{2}}\frac{1}{\sqrt{\vec{\tilde{k}}_\perp^2+\tilde{m}^2}} \times \begin{pmatrix} \tilde{k}^L & \tilde{m} \\ -\tilde{m} & \tilde{k}^R \end{pmatrix}, \quad \text{such that their product}$$

$$\tilde{\mathcal{S}}\tilde{\mathcal{S}}'^{\dagger} = \frac{1}{2\sqrt{\vec{k}_\perp^2+\tilde{m}^2}\sqrt{\vec{\tilde{k}}_\perp^2+\tilde{m}^2}}\begin{pmatrix} C & \tilde{m}\Delta_\perp^R x \\ -\tilde{m}\Delta_\perp^L x & C^* \end{pmatrix}, \tag{B29}$$

where we use the shorthand $C(x,\vec{k}_\perp) \equiv \vec{k}_\perp \cdot \vec{\tilde{k}}_\perp - ix(\vec{\Delta} \times \vec{k}_\perp)_z + \tilde{m}^2$ and $\vec{\tilde{k}} = \vec{k}_\perp - x\vec{\Delta}_\perp$ is defined in the same way as in Eq. (B18). The matrix $U^{\mu\nu}$ transforms as

$$\begin{aligned} U^{\mu\nu}_{\lambda'_q\lambda_q} &\to \frac{1}{4(1-x)}\bar{u}_{\lambda'_q}(p'_{\bar{q}})[\gamma^\mu p^\nu_{s\bar{q}} + \gamma^\nu p^\mu_{s\bar{q}}]u_{\lambda_q}(p_{\bar{q}}) \\ &= \frac{1}{4(1-x)}\bar{v}_{\lambda_q}(p_{\bar{q}})[\gamma^\mu p^\nu_{s\bar{q}} + \gamma^\nu p^\mu_{s\bar{q}}]v_{\lambda'_q}(p'_{\bar{q}}) = V^{\mu\nu}_{\lambda_q\lambda'_q}, \end{aligned} \tag{B30}$$

where to get the last line we use the spinor identity [74] $\bar{u}_{\lambda'_q}(p'_{\bar{q}})\gamma^\mu u_{\lambda_q}(p_{\bar{q}}) = \bar{v}_{\lambda_q}(p_{\bar{q}})\gamma^\mu v_{\lambda'_q}(p'_{\bar{q}})$. The transformed quark contribution to the matrix element with the renaming of the dummy summation variables $\lambda_q \to \lambda_{\bar{q}}$, $\lambda'_q \to \lambda'_{\bar{q}}$, and $\lambda_2 \to \lambda_1$ becomes

$$\begin{aligned} \langle \hat{T}^{\mu\nu}_q(m_q \leftrightarrow m_{\bar{q}})\rangle &= \int \frac{dx\, d^2\vec{k}_\perp}{2(2\pi)^3}\varphi^*(x,\vec{\tilde{k}}_\perp)\varphi(x,\vec{k}_\perp) \\ &\quad \sum_{\lambda_{\bar{q}},\lambda'_{\bar{q}},\lambda_1} \tilde{\mathcal{S}}^*_{\lambda'_{\bar{q}}\lambda_1}(x,\vec{\tilde{k}}_\perp)V^{\mu\nu}_{\lambda_{\bar{q}}\lambda'_{\bar{q}}}\tilde{\mathcal{S}}_{\lambda_{\bar{q}}\lambda_1}(x,\vec{k}_\perp) \\ &= \int \frac{dx\, d^2\vec{k}_\perp}{2(2\pi)^3}\varphi^*(x,\vec{\tilde{k}}_\perp)\varphi(x,\vec{k}_\perp) \\ &\quad \times \mathrm{Tr}[\tilde{\mathcal{S}}^{*\prime}\mathcal{S}^T V^{\mu\nu}]. \end{aligned} \tag{B31}$$

The antiquark contribution to the matrix element from Eqs. (B17) and (B18) is expressed as,

$$\langle \hat{T}^{\mu\nu}_{\bar{q}}\rangle = \int \frac{dx\, d^2\vec{k}_\perp}{2(2\pi)^3}\varphi^*(x,\vec{\tilde{k}}_\perp)\varphi(x,\vec{k}_\perp) \times \mathrm{Tr}[\bar{\mathcal{S}}'^{\dagger}\mathcal{S}V^{\mu\nu}], \tag{B32}$$

where we have $\bar{\mathcal{S}}' = \mathcal{S}(x, \vec{\tilde{k}}_\perp = \vec{k}_\perp - x\vec{\Delta}_\perp)$. Now, writing explicitly the product of the spin wave functions occurring

in the right-hand side of the Eq. (B32),

$$\bar{\mathcal{S}}'^{\dagger}\mathcal{S} = \frac{1}{2\sqrt{\vec{k}_\perp^2+\tilde{m}^2}\sqrt{\vec{\tilde{k}}_\perp^2+\tilde{m}^2}} \times \begin{pmatrix} C & -\tilde{m}\Delta_\perp^L x \\ \tilde{m}\Delta_\perp^R x & C^* \end{pmatrix},$$

$$\text{where}, \quad \bar{\mathcal{S}}'^{\dagger} = \frac{1}{\sqrt{2}} \frac{1}{\sqrt{\vec{\tilde{k}}_\perp^2+\tilde{m}^2}} \begin{pmatrix} -k'^L & \tilde{m} \\ -\tilde{m} & -k'^R \end{pmatrix}. \tag{B33}$$

Using Eqs. (B29) and (B33) we get $[\tilde{\mathcal{S}}\tilde{\mathcal{S}}'^{\dagger}]^T = \tilde{\mathcal{S}}^{*\prime}\tilde{\mathcal{S}}^T = \bar{\mathcal{S}}'^{\dagger}\mathcal{S}$, which along with Eqs. (B31) and (B32) proves $\langle \hat{T}^{\mu\nu}_{\bar{q}} \rangle = \langle \hat{T}^{\mu\nu}_{q}(m_q \leftrightarrow m_{\bar{q}}) \rangle$. In the case of the symmetric mass system we have $\langle \hat{T}^{\mu\nu}_{\bar{q}} \rangle = \langle \hat{T}^{\mu\nu}_{q} \rangle$.

APPENDIX C: BT CONSTRUCTION AND DIFFERENT EXPRESSION OF A AND D TERM

The Lorentz decomposition of the matrix element of EMT for the spin-0 mesons is given by

$$T^{\mu\nu} = \Gamma_A^{\mu\nu} A + \Gamma_D^{\mu\nu} D, \tag{C1}$$

where we have $\Gamma_A^{\mu\nu} = 2\bar{P}^\mu \bar{P}^\nu$ and $\Gamma_D^{\mu\nu} = \frac{\Delta^\mu \Delta^\nu - g^{\mu\nu}\Delta^2}{2}$. While Eq. (C1) as it stands is generally valid, as we have discussed in Sec. II B, the manifest Lorentz covariance is lost in the phenomenological LFQM used in the present work. This, in turn, means that one can extract the GFFs from different components of $T^{\mu\nu}$, and their expression may differ depending on the component of EMT used to extract them. The Eq. (C1) gives us the following seven independent equations in a frame with $\Delta^+ = 0$ [55],

$$T^{++} = \Gamma_A^{++} A, \tag{C2}$$

$$T^{+-} = \Gamma_A^{+-} A + \Gamma_D^{+-} D, \tag{C3}$$

$$\Delta_\perp^i T^{+i} = \Delta_\perp^i \Gamma_A^{+i} A, \tag{C4}$$

$$\Delta_\perp^i \Delta_\perp^j T^{ij} = \Delta_\perp^i \Delta_\perp^i \Gamma_A^{ij} A, \tag{C5}$$

$$T^{ii} = \Gamma_A^{ii} A + \Gamma_D^{ii} D, \tag{C6}$$

$$\Delta_\perp^i T^{-i} = \Delta_\perp^i \Gamma_A^{-i} A + \Delta_\perp^i \Gamma_D^{-i} D, \tag{C7}$$

$$T^{--} = \Gamma_A^{--} A + \Gamma_D^{--} D, \tag{C8}$$

where we used $\Gamma_D^{++} = \Gamma_D^{+i} = \Delta_\perp^i \Delta_\perp^j \Gamma_D^{ij} = 0$. One sees that A-term can be obtained in three independent ways using Eqs. (C2), (C4), or (C5) irrespective of D. Moreover, once one determines A, then D can be evaluated independently using either Eqs. (C3), (C6), (C7) or (C8). Let us write down the expressions of the A-term evaluated in this way with the BT construction applied only to the matrix element,

$$A^{(++)} = \frac{T^{++}}{\Gamma_A^{++}} = \frac{1}{2(P^+)^2} \int_\phi S^{++}, \tag{C9}$$

$$A^{(+i)} = \frac{\Delta_\perp^i T^{+i}}{\Delta_\perp^i \Gamma_A^{+i}} = \frac{1}{P^+ \vec{\Delta}_\perp^2} \int_\phi \Delta_\perp^i S^{+i}, \tag{C10}$$

$$A^{(ij)} = \frac{\Delta_\perp^i \Delta_\perp^i T^{ij}}{\Delta_\perp^i \Delta_\perp^j \Gamma_A^{ij}} = \frac{2}{\vec{\Delta}_\perp^4} \int_\phi \Delta_\perp^i \Delta_\perp^j S^{ij}, \tag{C11}$$

where the integral $\int_\phi \equiv \int \frac{dx d^2\vec{k}_\perp}{2(2\pi)^3} \varphi^*(x, \vec{k}'_\perp)\varphi(x, \vec{k}_\perp)$. One can also define the integrands that lead to the corresponding expression of A-term in Eqs. (C9)–(C11) as, $A^{(**)} = \int_\phi \mathcal{A}^{(**)}$, where $(**) \in \{++, +i, ij\}$. Now, since D can be evaluated in four independent ways, and each of the Eqs. (C3), (C6)–(C8) contains A, we obtain twelve independent expressions for D,

$$D^{(+-)}_{(**)} = \frac{T^{+-}}{\Gamma_D^{+-}} - \frac{\Gamma_A^{+-}}{\Gamma_D^{+-}} A^{(**)} = \frac{1}{\vec{\Delta}_\perp^2} \int_\phi S^{+-} - \frac{2M^2 + \vec{\Delta}_\perp^2}{\vec{\Delta}_\perp^2} \int_\phi \mathcal{A}^{(**)}, \tag{C12}$$

$$D^{(ii)}_{(**)} = \frac{T^{ii}}{\Gamma_D^{ii}} - \frac{\Gamma_A^{ii}}{\Gamma_D^{ii}} A^{(**)} = -\frac{2}{\vec{\Delta}_\perp^2} \int_\phi S^{ii} + \int_\phi \mathcal{A}^{(**)}, \tag{C13}$$

$$D^{(-i)}_{(**)} = \frac{\Delta_\perp^i T^{-i}}{\Delta_\perp^i \Gamma_D^{-i}} - \frac{\Delta_\perp^i \Gamma_A^{-i}}{\Delta_\perp^i \Gamma_D^{-i}} A^{(**)} = \frac{2P^+}{\vec{\Delta}_\perp^4} \int_\phi \Delta_\perp^i S^{-i} - \frac{2M^2 + \vec{\Delta}_\perp^2}{\vec{\Delta}_\perp^2} \int_\phi \mathcal{A}^{(**)}, \tag{C14}$$

$$D^{(--)}_{(**)} = \frac{T^{--}}{\Gamma_D^{--}} - \frac{\Gamma_A^{--}}{\Gamma_D^{--}} A^{(**)} = \frac{2(P^+)^2}{\vec{\Delta}_\perp^4} \int_\phi S^{--} - \frac{(2M^2 + \vec{\Delta}_\perp^2)^2}{\vec{\Delta}_\perp^4} \int_\phi \mathcal{A}^{(**)}, \tag{C15}$$

where M is the physical mass of the meson. In arriving at Eqs. (C12)–(C15) we used the explicit expression of the Lorentz structures $\Gamma_A^{\mu\nu}$ and $\Gamma_D^{\mu\nu}$.

Within the ambit of the BT construction, as discussed in Sec. II B, the form of the $\Gamma_A^{\mu\nu}$ changes and the physical meson mass is replaced with the invariant mass. Therefore, the meson mass associated with in the initial P and final momentum P' differs, i.e., $P^2 = M_0^2$ and $P'^2 = M_0'^2$. The modification of the Lorentz structures is provided in Table III. We write the different expressions of A and D-terms within the BT framework using Eqs. (C2)–(C8) and Table III as

TABLE III. The modifications of the Lorentz structure in the presence of BT construction.

$(\mu\nu)$	$\Gamma_A^{\mu\nu}\vert_{\rm BT}$	$\Gamma_D^{\mu\nu}\vert_{\rm BT}$
$(++)$	$2(P^+)^2$	0
$(+-)$	$2M_0'^2+\vec{\Delta}_\perp^2$	$\vec{\Delta}_\perp^2$
$(+i)$	$P^+\Delta_\perp^i(1+\frac{M_0'^2-M_0^2}{\vec{\Delta}_\perp^2})$	0
(ij)	$\frac{1}{2}[\Delta_\perp^i\Delta_\perp^j(1+\frac{2(M_0'^2-M_0^2)}{\vec{\Delta}_\perp^2})+\frac{(M_0'^2-M_0^2)^2}{\vec{\Delta}_\perp^2}\delta^{ij}]$	$\frac{1}{2}(\Delta_\perp^i\Delta_\perp^j-\delta^{ij}\vec{\Delta}_\perp^2)$
$(-i)$	$\frac{(2M_0'^2+\vec{\Delta}_\perp^2)(M_0'^2-M_0^2+\vec{\Delta}_\perp^2)\Delta_\perp^i}{2\vec{\Delta}_\perp^2P^+}$	$\frac{M_0'^2-M_0^2+\vec{\Delta}_\perp^2}{2P^+}\Delta_\perp^i$
$(--)$	$\frac{(M_0'^2+M_0^2+\vec{\Delta}_\perp^2)(\vec{\Delta}_\perp^2(M_0'^2+M_0^2+\vec{\Delta}_\perp^2)+2(M_0'^2-M_0^2)(M_0'^2-M_0^2+\vec{\Delta}_\perp^2))}{2(P^+)^2\vec{\Delta}_\perp^2}$	$\frac{(M_0'^2-M_0^2+\vec{\Delta}_\perp^2)^2}{2(P^+)^2}$

$$A^{(++)}|_{\rm BT}=\frac{T^{++}}{\Gamma_A^{++}}\bigg|_{\rm BT}=\int_\phi\frac{S^{++}}{2(P^+)^2},\tag{C16}$$

$$A^{(+i)}|_{\rm BT}=\frac{\Delta_\perp^iT^{+i}}{\Delta_\perp^i\Gamma_A^{+i}}\bigg|_{\rm BT}=\int_\phi\frac{\Delta_\perp^iS^{+i}}{P^+(M_0'^2-M_0^2+\vec{\Delta}_\perp^2)},\tag{C17}$$

$$A^{(ij)}|_{\rm BT}=\frac{\Delta_\perp^i\Delta_\perp^iT^{ij}}{\Delta_\perp^i\Delta_\perp^j\Gamma_A^{ij}}|_{\rm BT}=\int_\phi\frac{2\Delta_\perp^i\Delta_\perp^jS^{ij}}{\vec{\Delta}_\perp^4+(M_0'^2-M_0^2)(M_0'^2-M_0^2+2\vec{\Delta}_\perp^2)},\tag{C18}$$

$$D_{(**)}^{(+-)}|_{\rm BT}=\frac{T^{+-}}{\Gamma_D^{+-}}-\frac{\Gamma_A^{+-}}{\Gamma_D^{+-}}A^{(**)}|_{\rm BT}=\int_\phi\frac{S^{+-}}{\vec{\Delta}_\perp^2}-\int_\phi\frac{2M_0'^2+\vec{\Delta}_\perp^2}{\vec{\Delta}_\perp^2}\mathcal{A}^{(**)}|_{\rm BT},\tag{C19}$$

$$D_{(**)}^{(ii)}|_{\rm BT}=\frac{T^{ii}}{\Gamma_D^{ii}}-\frac{\Gamma_A^{ii}}{\Gamma_D^{ii}}A^{(**)}|_{\rm BT}=-\int_\phi\frac{2S^{ii}}{\vec{\Delta}_\perp^2}+\int_\phi\mathcal{A}^{(**)}|_{\rm BT}\times\frac{\vec{\Delta}_\perp^4+2(M_0'^2-M_0^2)(\vec{\Delta}_\perp^2+M_0'^2-M_0^2)}{\vec{\Delta}_\perp^4},\tag{C20}$$

$$D_{(**)}^{(-i)}|_{\rm BT}=\frac{\Delta_\perp^iT^{-i}}{\Delta_\perp^i\Gamma_D^{-i}}-\frac{\Delta_\perp^i\Gamma_A^{-i}}{\Delta_\perp^i\Gamma_D^{-i}}A^{(**)}|_{\rm BT}=\int_\phi\frac{2P^+\Delta_\perp^iS^{-i}}{(M_0'^2-M_0^2+\vec{\Delta}_\perp^2)\vec{\Delta}_\perp^2}-\int_\phi\frac{2M_0'^2+\vec{\Delta}_\perp^2}{\vec{\Delta}_\perp^2}\mathcal{A}^{(**)}|_{\rm BT},\tag{C21}$$

$$D_{(**)}^{(--)}|_{\rm BT}=\frac{T^{--}}{\Gamma_D^{--}}-\frac{\Gamma_A^{--}}{\Gamma_D^{--}}A^{(**)}|_{\rm BT}=\int_\phi\frac{2(P^+)^2S^{--}}{(M_0'^2-M_0^2+\vec{\Delta}_\perp^2)^2}-\int_\phi\mathcal{A}^{(**)}|_{\rm BT}\bigg[\frac{(M_0'^2+M_0^2+\vec{\Delta}_\perp^2)^2}{(M_0'^2-M_0^2+\vec{\Delta}_\perp^2)^2}+\frac{2(M_0'^2-M_0^2)(M_0'^2+M_0^2+\vec{\Delta}_\perp^2)}{\vec{\Delta}_\perp^2(M_0'^2-M_0^2+\vec{\Delta}_\perp^2)}\bigg].\tag{C22}$$

In Fig. 7, we show the different extraction of the A-term using Eqs. (C9)–(C11) (shown by scattered points) and Eqs. (C16)–(C18) (shown in continuous lines). Interestingly, we observe that the results of the five extractions merge, while one extraction, $A^{(ij)}$, shows a divergent trend at low momentum transfer. This demonstrates that the (ij) component should be avoided in extracting the A-term without a proper implementation of the BT construction in LFQM. Similarly, we show different extractions of the D-term sector-wise (we are identifying the superscripts of D in Eqs. (C12)–(C15) or Eqs. (C19)–(C22) as sectors) in Figs. 8–10, for $(+-)$, $(-i)$, and (ii) sectors, respectively. In all these plots, we observe that after BT implementation, the D-term results for quarkonia with two different wave functions remain the same. An improper application of BT construction, i.e., only for the matrix elements, leads to different magnitudes for D-terms, which not only depend upon the sector chosen but also on the A used to extract them. For the sector $(--)$ (not shown in the paper), we verified that even BT construction cannot cure the zero-mode contribution, and the extracted D differs. This extends the conclusion of Ref. [55] in reference to the pion for the quarkonia.

APPENDIX D: DIFFERENT SPATIAL DENSITIES FROM EMT

Here we collect some of the formulas that are discussed in several references [3,69] for the sake of completeness.

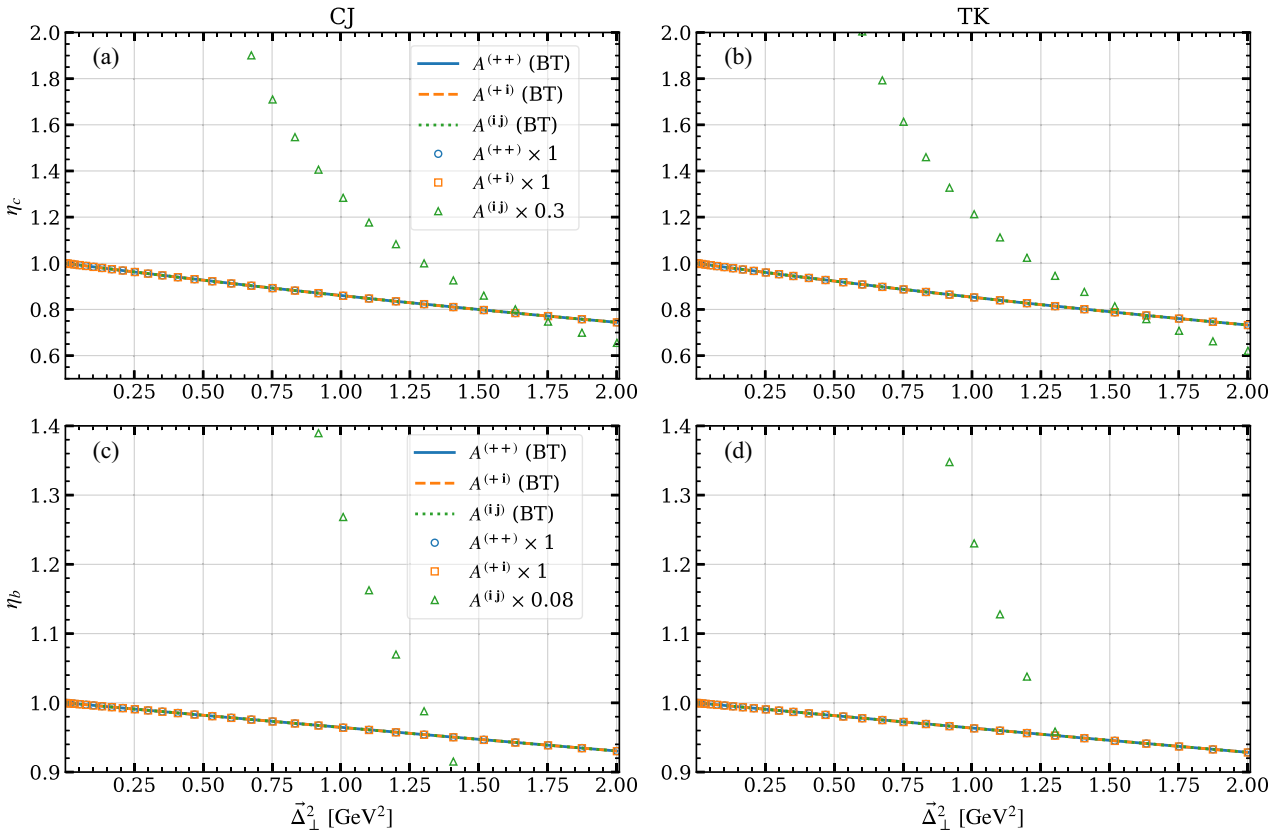


FIG. 7. Different extraction of A-term for η_c (upper panel) and η_b (lower panel) with different radial wave functions CJ (left) and TK (right). Figures in the upper panel [(a) and (b)] share the same legend [the same is true for Figs. (c) and (d)].

Before doing so, we will briefly explain how the light front densities are defined with the help of wave packets closely following Ref. [69]. Let us start with the definition of the spatial densities as provided in Ref. [69],

$$\int dz^- \langle\psi|\hat{T}^{\mu\nu}(z^+=0,z^-,\vec{z}_\perp)|\psi\rangle = 2\pi(2\sigma)^2 \int \frac{d^2\vec{P}_\perp}{(2\pi)^2} e^{-2\sigma^2\vec{P}_\perp^2} \int \frac{d^2\vec{\Delta}_\perp}{(2\pi)^2 2P^+} \langle\hat{T}^{\mu\nu}(0)\rangle e^{-i\vec{\Delta}_\perp\cdot\vec{z}_\perp} e^{-\sigma^2\vec{\Delta}_\perp^2/2}. \tag{D1}$$

The left-hand side of Eq. (D1) gives the definition of the spatial density associated with an operator (in our case, the EMT operator) in a localized meson state $|\psi\rangle$. Note that the $|\psi\rangle$ here is different from the Ψ defined in Sec. II A; Ψ was used for the distribution of the quarks inside a plane wave state of the meson, whereas the $|\psi\rangle$ here is the meson wave packet made up of the plane wave states. To get the right-hand side of Eq. (D1), the wave packet is chosen in the momentum space so that it has a given momentum in the longitudinal direction, i.e., P^+, but is localized (spatially) in the perpendicular direction with a finite width σ [69]. Note that a spatially localized wave packet is needed to make the description of density meaningful. To get the density in an arbitrarily localized wave packet in the transverse plane, one needs to take the limit $\sigma \to 0$ after all the integrals in the right-hand side of Eq. (D1) are performed. Since one has to get rid of the width of the wave packet to have meaningful internal density, the matrix elements between the plane wave states $\langle\hat{T}^{\mu\nu}(0)\rangle$ should not have $\vec{P}_\perp$ dependence [69]. From Eq. (15) we notice that only the matrix element $\langle\hat{T}^{++}(0)\rangle$ and $\langle\hat{T}^{ij}(0)\rangle$ has no $\vec{P}$ dependence. For such matrix elements the $\vec{P}_\perp$ integral in Eq. (D1) can be done resulting,

$$\int dz^- \langle\psi|\hat{T}^{\mu\nu}(z^+=0,z^-,\vec{z}_\perp)|\psi\rangle = \int \frac{d^2\vec{\Delta}_\perp}{(2\pi)^2 2P^+} \langle\hat{T}^{\mu\nu}(0)\rangle e^{-i\vec{\Delta}_\perp\cdot\vec{z}_\perp} e^{-\sigma^2\vec{\Delta}_\perp^2/2}. \tag{D2}$$

Now it is trivially seen that the shear tensor defined in Eq. (16) and the LF momentum density defined in Eq. (23) are actually the density associated with $\langle\hat{T}^{ij}(0)\rangle$ and $\langle\hat{T}^{++}(0)\rangle$, respectively, in the limit $\sigma \to 0$. We proceed from here to prove Eqs. (19) and (18), which define the pressure and shear function. The LF pure stress tensor is given by

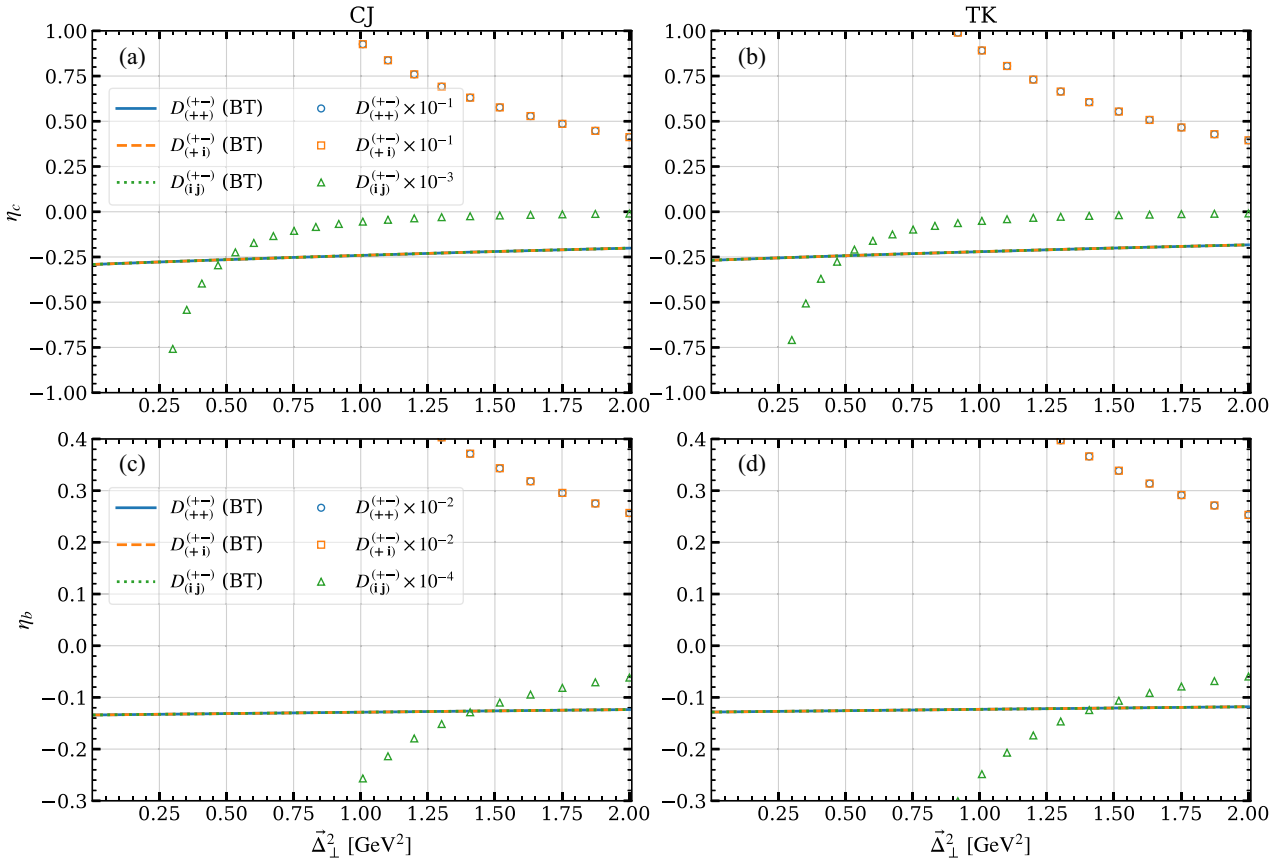


FIG. 8. Different extraction of D-term in the $(+-)$ sector for η_c (upper panel) and η_b (lower panel) with different radial wave functions CJ (left) and TK (right). Figures in the upper panel [(a) and (b)] share the same legend [the same is true for Figs. (c) and (d)].

$$S^{ij} = \frac{1}{4P^+}\int \frac{d^2\vec{\Delta}_\perp}{(2\pi)^2} e^{-i\vec{\Delta}_\perp\cdot\vec{z}_\perp}(\Delta^i_\perp\Delta^j_\perp - \vec{\Delta}^2_\perp\delta^{ij})D$$
$$= \frac{1}{4P^+}\int \frac{d^2\vec{\Delta}_\perp}{(2\pi)^2} D(-\partial_i\partial_j + \delta^{ij}\partial^2)e^{-i\vec{\Delta}_\perp\cdot\vec{z}_\perp}$$
$$= (-\partial_i\partial_j + \delta^{ij}\partial^2)\tilde{D}, \tag{D3}$$

where we define $\partial_i = \partial/\partial z^i_\perp$, $\partial^2 = \partial_i\partial_i$ and δ^{ij} is the usual Kronecker delta. Note that we only assume that all the repeated indices are summed over and not following the known covariant-contravariant index prescription. It is useful to notice that the $\tilde{D}$ is only a function of $z_\perp = |\vec{z}_\perp|$ since D-term is isotropic, i.e., $D = D(-\vec{\Delta}^2_\perp)$. In fact, any Fourier transform of this type can be cast as an integration over the Bessel function of the first kind. To see this, let us recall that the generating function of the Bessel function of the first kind is given by $e^{\frac{x}{2}(t-\frac{1}{t})} = \sum_{n=-\infty}^{n=\infty} J_n(x)t^n$ and identifying $x = \Delta_\perp z_\perp$ and $t = -ie^{i\phi}$, where $\vec{\Delta}_\perp\cdot\vec{z}_\perp = \Delta_\perp z_\perp\cos\phi$, we have

$$\tilde{D} = \frac{1}{4P^+}\times\frac{1}{2\pi}\int_0^\infty D\,J_0(\Delta_\perp z_\perp)\Delta_\perp d\Delta_\perp. \tag{D4}$$

By exploiting the isotropic nature of $\tilde{D}$, Eq. (D3) can be further simplified by converting the transverse plane derivatives to radial derivatives in the transverse plane,

$$\partial_i\partial_j = -\left(\frac{z^i_\perp z^j_\perp}{z^2_\perp} - \delta^{ij}\right)\frac{1}{z_\perp}\frac{d}{dz_\perp} + \frac{z^i_\perp z^j_\perp}{z^2_\perp}\frac{d^2}{dz^2_\perp}, \tag{D5}$$

$$\partial^2 = \frac{1}{z_\perp}\frac{d}{dz_\perp} + \frac{d^2}{dz^2_\perp}. \tag{D6}$$

Substituting the Eqs. (D5) and (D6) in Eq. (D3) with a bit of rearrangement we have

$$S^{ij} = \left[\left(\frac{z^i_\perp z^j_\perp}{z^2_\perp} - \frac{1}{2}\delta^{ij}\right)\left(\frac{1}{z_\perp}\frac{d}{dz_\perp} - \frac{d^2}{dz^2_\perp}\right) + \delta^{ij}\left(\frac{1}{2z_\perp}\frac{d}{dz_\perp} + \frac{1}{2}\frac{d^2}{dz^2_\perp}\right)\right]\tilde{D}. \tag{D7}$$

Comparing Eq. (D7) with Eq. (17), we obtain the pressure and shear function as defined in Eqs. (19) and (18). Since pressure and shear function are obtained from the same function $\tilde{D}$, they are not independent. One can straightforwardly show from the definition (D3) of the shear stress

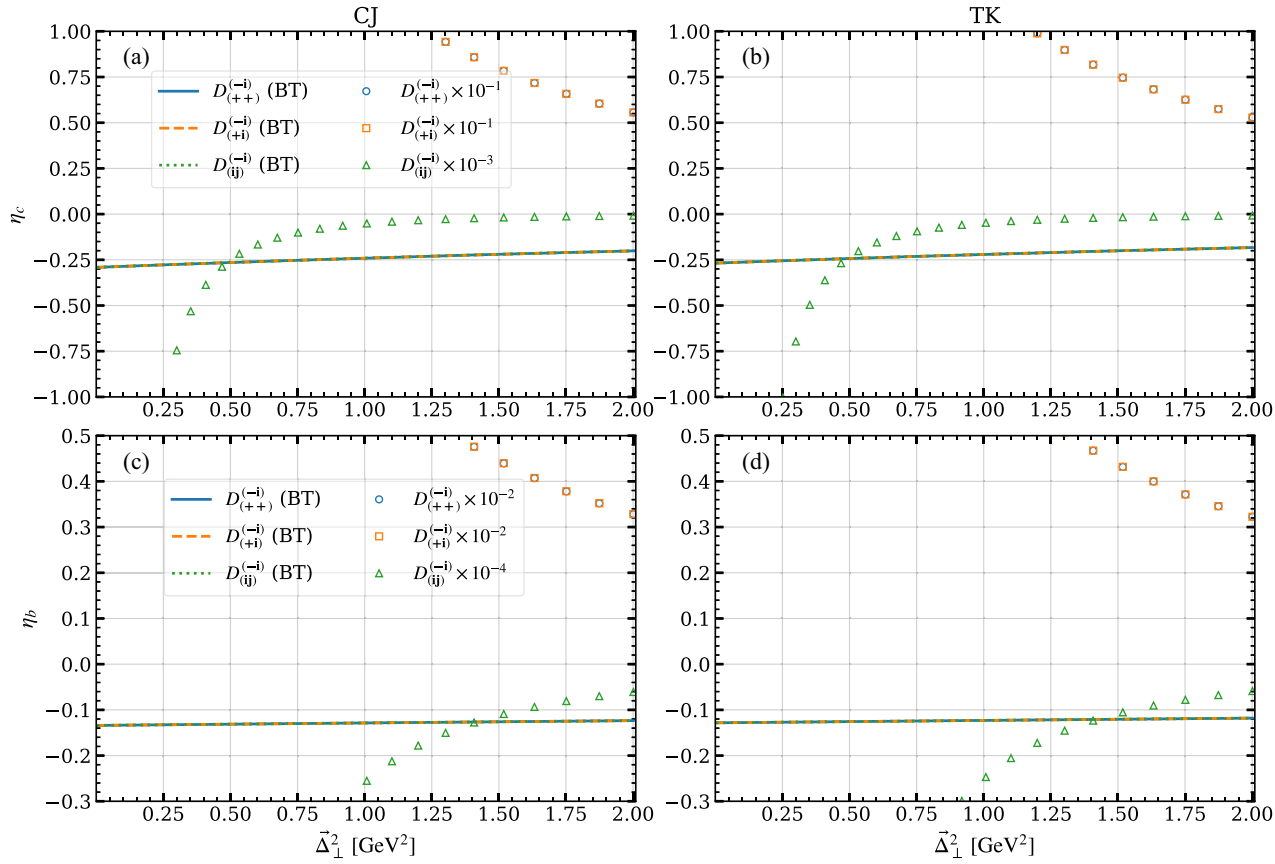


FIG. 9. Different extraction of D-term in the $(-i)$ sector for η_c (upper panel) and η_b (lower panel) with different radial wave functions CJ (left) and TK (right). Figures in the upper panel [(a) and (b)] share the same legend [the same is true for Figs. (c) and (d)].

that it is conserved, i.e., $\partial_i S^{ij} = \partial_i(-\partial_i\partial_j + \delta^{ij}\partial^2)\tilde{D} = 0$. Equation (21) can be shown to hold directly from the definitions of pressure and shear functions provided in Eq. (D7) or from the shear stress conservation. From the conservation of the shear stress, we have

$$\begin{aligned}
&\partial_i\left[\left(\frac{z_\perp^i z_\perp^j}{z_\perp^2} - \frac{\delta^{ij}}{2}\right)s(z_\perp) + \delta^{ij}p(z_\perp)\right] = 0 \\
&\text{or,} \quad \left(\frac{z_\perp^i z_\perp^j}{z_\perp^2} - \frac{\delta^{ij}}{2}\right)\partial_i s(z_\perp) + s(z_\perp)\partial_i\left(\frac{z_\perp^i z_\perp^j}{z_\perp^2} - \frac{\delta^{ij}}{2}\right) \\
&\quad + \delta^{ij}\partial_i p(z_\perp) = 0 \\
&\text{or,} \quad s'\frac{z_\perp^i}{z_\perp}\left(\frac{z_\perp^i z_\perp^j}{z_\perp^2} - \frac{\delta^{ij}}{2}\right) + s(z_\perp)\frac{z_\perp^j}{z_\perp^2} + p'\frac{z_\perp^j}{z_\perp} = 0 \\
&\text{or,} \quad \frac{1}{2}s'\frac{z_\perp^j}{z_\perp} + s(z_\perp)\frac{z_\perp^j}{z_\perp^2} + p'\frac{z_\perp^j}{z_\perp} = 0 \\
&\text{or,} \quad \frac{1}{2}s' + s(z_\perp)\frac{1}{z_\perp} + p' = 0, \qquad \text{(D8)}
\end{aligned}$$

where we used $\frac{\partial}{\partial z_i} = \frac{z_\perp^i}{z_\perp}\frac{d}{dz_\perp}$, $p' \equiv \frac{dp}{dz_\perp}$ and $s' \equiv \frac{ds}{dz_\perp}$. Equation (D8) is in agreement with Eq. (21). To obtain the second equality [Eq. (22)], which is the von Laue stability criterion, we first rewrite the pressure in a different way using Eq. (D3),

$$p(z_\perp) = \frac{1}{2}S^{ij}\delta^{ij} = \frac{-1}{8P^+}\int\frac{d^2\vec{\Delta}_\perp}{(2\pi)^2}\Delta_\perp^2 D e^{-i\vec{\Delta}_\perp\cdot\vec{z}_\perp}. \qquad \text{(D9)}$$

From Eq. (D9), we get the von Laue stability condition by directly integrating in the transverse space as follows

$$\begin{aligned}
\int d^2\vec{z}_\perp\, p(z_\perp) &= \frac{-1}{8P^+}\int d^2\vec{\Delta}_\perp\Delta_\perp^2 D\int\frac{d^2\vec{z}_\perp}{(2\pi)^2}e^{-i\vec{\Delta}_\perp\cdot\vec{z}_\perp} \\
&= \frac{-1}{8P^+}\int d^2\vec{\Delta}_\perp\Delta_\perp^2 D\delta^2(\vec{\Delta}_\perp) \\
&= 0, \qquad \text{(D10)}
\end{aligned}$$

where we use $\lim_{\vec{\Delta}_\perp\to 0}\Delta_\perp^2 D(-\Delta_\perp^2) = 0$. We can also find out the moment of the pressure and shear function by using their definitions in Eq. (20) and repeatedly applying integration by parts,

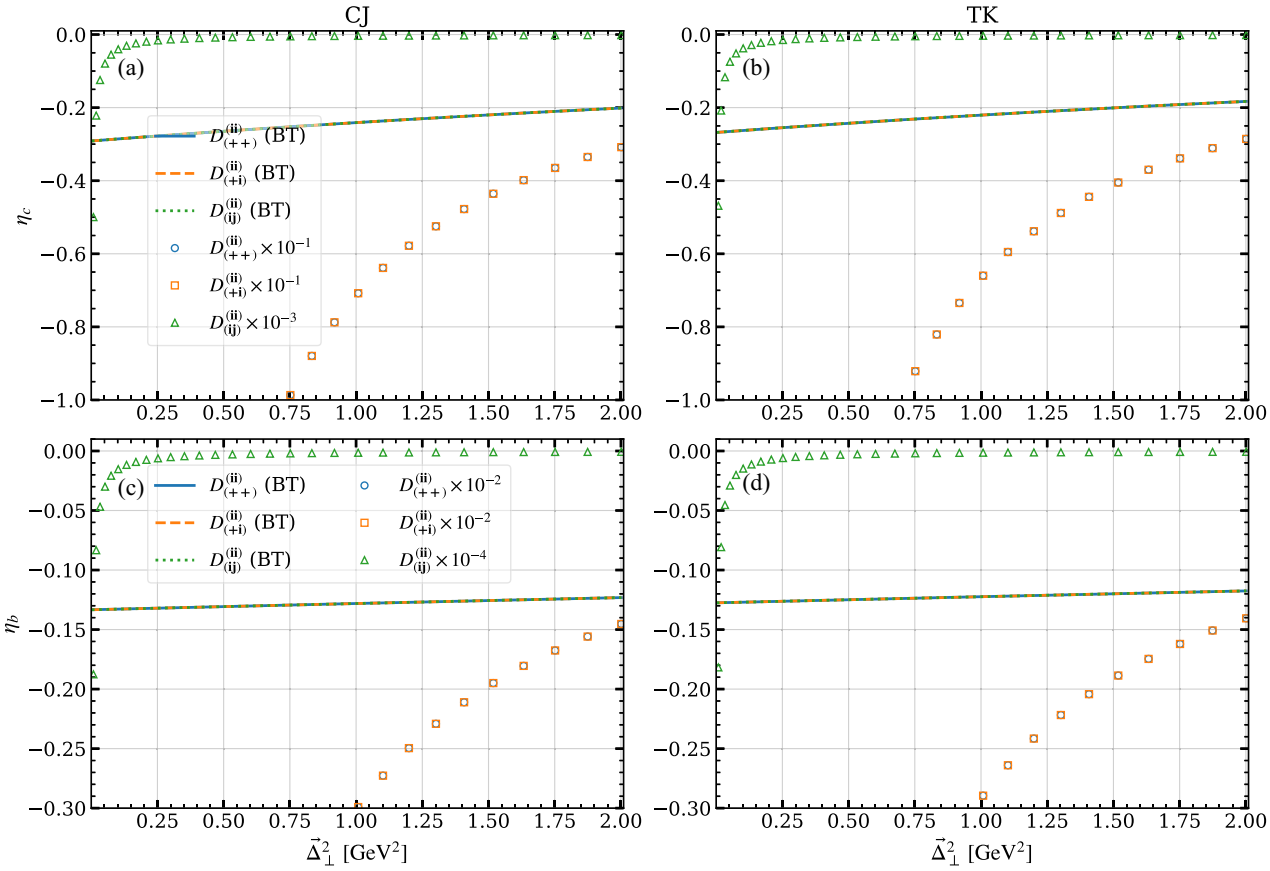


FIG. 10. Different extraction of D-term in the (ii) sector for η_c (upper panel) and η_b (lower panel) with different radial wave functions CJ (left) and TK (right). Figures in the upper panel [(a) and (b)] share the same legend [the same is true for Figs. (c) and (d)].

$$\begin{aligned}\int z_\perp^2 p(z_\perp) d^2\vec{z}_\perp &= 2\pi \int \frac{z_\perp^2}{2}\frac{d}{dz_\perp}\left(z_\perp \frac{d\tilde{D}}{dz_\perp}\right) dz_\perp \\ &= -2\pi \int z_\perp^2 \frac{d\tilde{D}}{dz_\perp} dz_\perp = 2\int \tilde{D} d^2\vec{z}_\perp \\ &= \int \frac{d^2\vec{\Delta}_\perp}{2P^+} D(-\vec{\Delta}_\perp^2) \int \frac{d^2\vec{z}_\perp}{(2\pi)^2} e^{-i\vec{\Delta}_\perp\cdot\vec{z}_\perp} \\ &= \frac{D(0)}{2P^+}, \end{aligned} \tag{D11}$$

where we assume that owing to the property of the $\tilde{D}$, the integrated part always vanishes at spatial infinity. Equation (D11) suggest that for any system having $D(0) < 0$, the $z_\perp^2$-weighted moment of pressure is negative. Similarly, it can be easily seen following the similar steps that lead to Eq. (D11),

$$\int z_\perp^2 s(z_\perp) d^2\vec{z}_\perp = \frac{-2D(0)}{P^+}. \tag{D12}$$

Equation (D12) states that for any system having $D(0) < 0$, the $z_\perp^2$-weighted moment of shear function is positive. Similarly, one can obtain the shear function integrated over the space,

$$\int s(z_\perp) d^2\vec{z}_\perp = \frac{-1}{4P^+}\int_{-\infty}^{0} D(t) dt, \tag{D13}$$

where $t \equiv -\vec{\Delta}_\perp^2$. Combining Eqs. (D10)–(D12), and (D13) the squared average mechanical radius defined in Eq. (26),

$$\begin{aligned}\langle z_\perp^2\rangle_{\mathscr{F}} &= \frac{\int d^2\vec{z}_\perp z_\perp^2 (p(z_\perp) + \frac{1}{2}s(z_\perp))}{\int d^2\vec{z}_\perp (p(z_\perp) + \frac{1}{2}s(z_\perp))} \\ &= \frac{4D(0)}{\int_{-\infty}^{0} D(t) dt}. \end{aligned} \tag{D14}$$

The squared average momentum radius defined in Eq. (25) is,

$$\begin{aligned}\langle z_\perp^2\rangle_{\mathcal{P}} &= \frac{1}{P^+}\int d^2\vec{z}_\perp z_\perp^2 \mathcal{P}(z_\perp) = \int \frac{d^2\vec{\Delta}_\perp}{(2\pi)^2} A \int d^2\vec{z}_\perp z_\perp^2 e^{-i\vec{\Delta}_\perp\cdot\vec{z}_\perp} \\ &= -\int d^2\vec{\Delta}_\perp A\delta^{ij}\frac{\partial^2}{\partial\Delta_\perp^i\partial\Delta_\perp^j}\int\frac{d^2\vec{z}_\perp}{(2\pi)^2}e^{-i\vec{\Delta}_\perp\cdot\vec{z}_\perp} \\ &= -\int d^2\vec{\Delta}_\perp A\delta^{ij}\frac{\partial^2\delta^2(\vec{\Delta}_\perp)}{\partial\Delta_\perp^i\partial\Delta_\perp^j} \\ &= -\int d^2\vec{\Delta}_\perp\delta^{ij}\frac{\partial^2 A(-\vec{\Delta}_\perp^2)}{\partial\Delta_\perp^i\partial\Delta_\perp^j}\delta^2(\vec{\Delta}_\perp) \\ &= -4\frac{dA}{d\vec{\Delta}_\perp^2}\Big|_{\vec{\Delta}_\perp^2=0} = 4\frac{dA}{dt}\Big|_{t=0} \end{aligned} \tag{D15}$$

where we integrated by parts to remove the derivatives from the delta function and used the identity $\delta^{ij}\frac{\partial^2 A}{\partial\Delta_\perp^i\partial\Delta_\perp^j} = 4\frac{dA}{d\vec{\Delta}_\perp^2} + 4\vec{\Delta}_\perp^2\frac{d^2A}{d^2\vec{\Delta}_\perp^2}$. The LF longitudinal momentum density integrated over all space, we get,

$$\begin{aligned}\int \mathcal{P}d^2\vec{z}_\perp &= P^+\int d^2\vec{\Delta}_\perp A(-\vec{\Delta}_\perp^2)\int\frac{d^2\vec{z}_\perp}{(2\pi)^2}e^{-i\vec{\Delta}_\perp\cdot\vec{z}_\perp} \\ &= P^+\int d^2\vec{\Delta}_\perp A(-\vec{\Delta}_\perp^2)\delta^2(\vec{\Delta}_\perp) \\ &= P^+A(0) \end{aligned} \tag{D16}$$

From which we can ascertain the sum rule $A(0) = 1$. The energy density on the LF turns out to be a compound density consisting of two parts: the barycentric kinetic energy density and the internal energy density [71]. Readers can see Ref. [71] to learn about compound density and their derivation. In Eq. (24) we have provided only the internal energy density. One can also express the internal energy density as

$$\begin{aligned}\mathcal{E} &= \frac{1}{2P^+}\left(M^2\tilde{A} - \frac{1}{4}\partial^2\tilde{A} - \frac{1}{2}\partial^2 4P^+\tilde{D}\right) \\ &= \frac{1}{2P^+}\left[M^2\tilde{A} - \frac{1}{4}\left(\frac{1}{z_\perp}\frac{d(\tilde{A}+4P^+\tilde{D})}{dz_\perp} + \frac{d^2(\tilde{A}+4P^+\tilde{D})}{dz_\perp^2}\right)\right]. \end{aligned} \tag{D17}$$

We close the discussion by commenting on the fact that if one assumes a 3D density obtained from the Fourier transformation and an associated form factor $\mathscr{F}(-\vec{\Delta}^2)$ following the similar steps as performed to obtain Eq. (D15), the mean squared radius is given by, $\langle r^2\rangle_{\mathscr{F}} = -6\frac{d\mathscr{F}}{d\Delta^2}|_{\Delta^2=0}$.

[1] V. D. Burkert, L. Elouadrhiri, and F. X. Girod, The pressure distribution inside the proton, Nature (London) **557**, 396 (2018).
[2] M. V. Polyakov, Generalized parton distributions and strong forces inside nucleons and nuclei, Phys. Lett. B **555**, 57 (2003).
[3] M. V. Polyakov and P. Schweitzer, Forces inside hadrons: Pressure, surface tension, mechanical radius, and all that, Int. J. Mod. Phys. A **33**, 1830025 (2018).
[4] V. D. Burkert, L. Elouadrhiri, F. X. Girod, C. Lorcé, P. Schweitzer, and P. E. Shanahan, Colloquium: Gravitational form factors of the proton, Rev. Mod. Phys. **95**, 041002 (2023).
[5] X.-D. Ji, Deeply virtual Compton scattering, Phys. Rev. D **55**, 7114 (1997).
[6] M. Burkardt, Impact parameter space interpretation for generalized parton distributions, Int. J. Mod. Phys. A **18**, 173 (2003).
[7] M. Diehl, Generalized parton distributions, Phys. Rep. **388**, 41 (2003).
[8] A. V. Belitsky and A. V. Radyushkin, Unraveling hadron structure with generalized parton distributions, Phys. Rep. **418**, 1 (2005).
[9] C. Lorcé, A. Metz, B. Pasquini, and P. Schweitzer, Parton distribution functions and their generalizations, Encycl. Part. Phys. **2**, 167 (2026).
[10] A. Accardi *et al.*, Electron ION collider: The next QCD frontier: Understanding the glue that binds us all, Eur. Phys. J. A **52**, 268 (2016).
[11] R. Abir *et al.*, The case for an EIC theory alliance: Theoretical Challenges of the EIC, arXiv:2305.14572.
[12] R. Abdul Khalek *et al.*, Science requirements and detector concepts for the electron-ion collider: EIC Yellow Report, Nucl. Phys. **A1026**, 122447 (2022).
[13] X. Ji, QCD analysis of the mass structure of the nucleon, Phys. Rev. Lett. **74**, 1071 (1995).
[14] K. Goeke, J. Grabis, J. Ossmann, M. V. Polyakov, P. Schweitzer, A. Silva, and D. Urbano, Nucleon form-factors of the energy momentum tensor in the chiral quark-soliton model, Phys. Rev. D **75**, 094021 (2007).
[15] C. Cebulla, K. Goeke, J. Ossmann, and P. Schweitzer, The Nucleon form-factors of the energy momentum tensor in the Skyrme model, Nucl. Phys. **A794**, 87 (2007).
[16] H.-C. Kim, P. Schweitzer, and U. Yakhshiev, Energy-momentum tensor form factors of the nucleon in nuclear matter, Phys. Lett. B **718**, 625 (2012).

[17] P. E. Shanahan and W. Detmold, Pressure distribution and shear forces inside the proton, Phys. Rev. Lett. **122**, 072003 (2019).
[18] C. Lorcé, H. Moutarde, and A. P. Trawiński, Revisiting the mechanical properties of the nucleon, Eur. Phys. J. C **79**, 89 (2019).
[19] D. Chakrabarti, C. Mondal, A. Mukherjee, S. Nair, and X. Zhao, Gravitational form factors and mechanical properties of proton in a light-front quark-diquark model, Phys. Rev. D **102**, 113011 (2020).
[20] X. Ji and Y. Liu, Momentum-current gravitational multipoles of hadrons, Phys. Rev. D **106**, 034028 (2022).
[21] A. Freese and G. A. Miller, Genuine empirical pressure within the proton, Phys. Rev. D **104**, 014024 (2021).
[22] M. Fujita, Y. Hatta, S. Sugimoto, and T. Ueda, Nucleon D-term in holographic quantum chromodynamics, Prog. Theor. Exp. Phys. **2022**, 093B06 (2022).
[23] P. Choudhary, B. Gurjar, D. Chakrabarti, and A. Mukherjee, Gravitational form factors and mechanical properties of the proton: Connections between distributions in 2D and 3D, Phys. Rev. D **106**, 076004 (2022).
[24] A. Garcia Martin-Caro, M. Huidobro, and Y. Hatta, Gravitational form factors of nuclei in the Skyrme model, Phys. Rev. D **108**, 034014 (2023).
[25] A. García Martín-Caro, M. Huidobro, and Y. Hatta, Nuclear mass radius and pressure in the Skyrme model, Phys. Rev. D **110**, 034002 (2024).
[26] D. C. Hackett, D. A. Pefkou, and P. E. Shanahan, Gravitational form factors of the Proton from Lattice QCD, Phys. Rev. Lett. **132**, 251904 (2024).
[27] X.-H. Cao, F.-K. Guo, Q.-Z. Li, and D.-L. Yao, Dispersive determination of nucleon gravitational form factors, Nat. Commun. **16**, 6979 (2025).
[28] S. Nair, C. Mondal, S. Xu, X. Zhao, A. Mukherjee, and J. P. Vary (BLFQ Collaboration), Gravitational form factors and mechanical properties of quarks in protons: A basis light-front quantization approach, Phys. Rev. D **110**, 056027 (2024).
[29] Y. Guo, F. Yuan, and W. Zhao, Bayesian inferring nucleon gravitational form factors via near-threshold J/ψ photoproduction, Phys. Rev. Lett. **135**, 111902 (2025).
[30] M. Goharipour, H. Hashamipour, H. Fatehi, F. Irani, K. Azizi, and S. V. Goloskokov (MMGPDs Collaboration), Mechanical properties of the nucleon from the generalized parton distributions, Phys. Rev. D **112**, 014016 (2025).
[31] X. Ji and C. Yang, Momentum flow mechanisms and color-lorentz forces on quarks in the nucleon, Research **9**, 1155 (2026).
[32] S. Sugimoto and T. Tsukamoto, Energy-momentum tensor and D-term of baryons in top-down holographic QCD, Prog. Theor. Exp. Phys. **2025**, 083B01 (2025).
[33] M. Tanaka, D. Fujii, and M. Kawaguchi, Gravitational form factors of the nucleon in the Skyrme model based on scale-invariant chiral perturbation theory, Phys. Rev. D **112**, 054048 (2025).
[34] X. Ji and C. Yang, A journey of seeking pressure and forces in the nucleon, Nucl. Phys. **B1024**, 117342 (2026).
[35] J. Deng and D. Hou, Proton structure from a soft-wall holographic QCD model: Mass spectrum, form factors, and mechanical properties, Eur. Phys. J. C **86**, 947 (2026).
[36] K. Fukushima and T. Uji, Pseudogauge ambiguity in the distributions of energy density, pressure, and shear force inside the nucleon, Phys. Rev. D **113**, 016025 (2026).
[37] K. Fukushima and T. Uji, Energy-momentum tensor form factors and spin density distribution in the nucleon calculated in a quantized Skyrme model with vector mesons, Phys. Rev. D **113**, 114049 (2026).
[38] J. Deng and D. Hou, Exploring nucleon structure and the proton mass problem through holographic QCD, Phys. Rev. D **114**, 026013 (2026).
[39] R. Stegeman and R. Zwicky, Gravitational D-form factor: The σ-meson as a dilaton confronted with lattice QCD data I, J. High Energy Phys. 03 (2026) 184.
[40] X.-H. Cao, F.-K. Guo, Q.-Z. Li, B.-W. Wu, and D.-L. Yao, Gravitational form factors of pions, kaons and nucleons from dispersion relations, Eur. Phys. J. Special Topics **235**, 2121 (2025).
[41] H.-Y. Won and C. Lorcé, Relativistic energy-momentum tensor distributions in a polarized nucleon, Phys. Rev. D **111**, 094021 (2025).
[42] H.-Y. Won and C. Lorcé, Transverse energy-momentum tensor distributions in polarized nucleons, Phys. Rev. D **114**, 014012 (2026).
[43] N. Kaur, S. Sharma, A. Jebarson A, and H. Dahiya, Mechanical properties of proton in the momentum space, Phys. Lett. B **879**, 140686 (2026).
[44] S. Nair, C. Mondal, S. Xu, X. Zhao, and J. P. Vary (BLFQ Collaboration), Proton gravitational structure and mass decomposition on the light front, Phys. Rev. D **112**, 114001 (2025).
[45] W. Broniowski and E. Ruiz Arriola, Gravitational and higher-order form factors of the pion in chiral quark models, Phys. Rev. D **78**, 094011 (2008).
[46] A. Freese and I. C. Cloët, Gravitational form factors of light mesons, Phys. Rev. C **100**, 015201 (2019); Phys. Rev. C **105**, 059901(E) (2022).
[47] W.-Y. Liu, E. Shuryak, and I. Zahed, Pion gravitational form factors in the QCD instanton vacuum. II, Phys. Rev. D **110**, 054022 (2024).
[48] W.-Y. Liu, E. Shuryak, C. Weiss, and I. Zahed, Pion gravitational form factors in the QCD instanton vacuum. I, Phys. Rev. D **110**, 054021 (2024).
[49] D. C. Hackett, P. R. Oare, D. A. Pefkou, and P. E. Shanahan, Gravitational form factors of the pion from lattice QCD, Phys. Rev. D **108**, 114504 (2023).
[50] A. F. Krutov and V. E. Troitsky, Pion gravitational form factors in a relativistic theory of composite particles, Phys. Rev. D **103**, 014029 (2021).
[51] Y.-Z. Xu, M. Ding, K. Raya, C. D. Roberts, J. Rodríguez-Quintero, and S. M. Schmidt, Pion and kaon electromagnetic and gravitational form factors, Eur. Phys. J. C **84**, 191 (2024).
[52] Y. Li and J. P. Vary, Stress inside the pion in holographic light-front QCD, Phys. Rev. D **109**, L051501 (2024).
[53] D. Fujii, A. Iwanaka, and M. Tanaka, Gravitational form factors of pion from top-down holographic QCD, Phys. Rev. D **110**, L091501 (2024).
[54] W. Broniowski and E. Ruiz Arriola, Gravitational form factors of the pion and meson dominance, Phys. Lett. B **859**, 139138 (2024).

[55] Y. Choi, H.-D. Son, and H.-M. Choi, Gravitational form factors of the pion in the self-consistent light-front quark model, Phys. Rev. D **112**, 014043 (2025).
[56] R. Stegeman and R. Zwicky, Gluon gravitational D-form factor: The σ-meson as a dilaton confronted with lattice data II, J. High Energy Phys. 05 (2026) 159.
[57] M. A. Sultan, Z. Xing, K. Raya, A. Bashir, and L. Chang, Gravitational form factors of pseudoscalar mesons in a contact interaction, Phys. Rev. D **110**, 054034 (2024).
[58] S. Xu, X. Cao, T. Hu, Y. Li, X. Zhao, and J. P. Vary, Gravitational form factors of charmonia, Phys. Rev. D **109**, 114024 (2024).
[59] T. Hu, X. Cao, S. Xu, Y. Li, X. Zhao, and J. P. Vary, Gravitational form factor D of charmonium from shear stress, Phys. Rev. D **111**, 074031 (2025).
[60] H.-M. Choi and C.-R. Ji, Mixing angles and electromagnetic properties of ground state pseudoscalar and vector meson nonets in the light cone quark model, Phys. Rev. D **59**, 074015 (1999).
[61] H.-M. Choi and C.-R. Ji, Self-consistent covariant description of vector meson decay constants and chirality-even quark-antiquark distribution amplitudes up to twist-3 in the light-front quark model, Phys. Rev. D **89**, 033011 (2014).
[62] H.-M. Choi and C.-R. Ji, Consistency of the light-front quark model with chiral symmetry in the pseudoscalar meson analysis, Phys. Rev. D **91**, 014018 (2015).
[63] H.-M. Choi and C.-R. Ji, Two-particle twist-3 distribution amplitudes of the pion and kaon in the light-front quark model, Phys. Rev. D **95**, 056002 (2017).
[64] H.-M. Choi, Self-consistent light-front quark model analysis of $B \to D\ell\nu_\ell$ transition form factors, Phys. Rev. D **103**, 073004 (2021).
[65] H.-M. Choi, Current-component independent transition form factors for semileptonic and rare D $\longrightarrow \pi$K decays in the light-front quark model, Adv. High Energy Phys. **2021**, 4277321 (2021).
[66] A. J. Arifi, H.-M. Choi, C.-R. Ji, and Y. Oh, Independence of current components, polarization vectors, and reference frames in the light-front quark model analysis of meson decay constants, Phys. Rev. D **107**, 053003 (2023).
[67] A. J. Arifi, H.-M. Choi, and C.-R. Ji, Pseudoscalar meson decay constants and distribution amplitudes up to the twist-4 in the light-front quark model, Phys. Rev. D **108**, 013006 (2023).
[68] H.-M. Choi and C.-R. Ji, Consistency of the pion form factor and unpolarized transverse momentum dependent parton distributions beyond leading twist in the light-front quark model, Phys. Rev. D **110**, 014006 (2024).
[69] A. Freese and G. A. Miller, Forces within hadrons on the light front, Phys. Rev. D **103**, 094023 (2021).
[70] A. Freese and G. A. Miller, Unified formalism for electromagnetic and gravitational probes: Densities, Phys. Rev. D **105**, 014003 (2022).
[71] A. Freese and G. A. Miller, Convolution formalism for defining densities of hadrons, Phys. Rev. D **108**, 034008 (2023).
[72] B.-Q. Ma, Spin structure of the pion in a light cone representation, Z. Phys. A **345**, 321 (1993).
[73] H.-M. Choi and C.-R. Ji, Relations among the light cone quark models with the invariant meson mass scheme and the model prediction of eta—eta-prime mixing angle, Phys. Rev. D **56**, 6010 (1997).
[74] S. J. Brodsky, H.-C. Pauli, and S. S. Pinsky, Quantum chromodynamics and other field theories on the light cone, Phys. Rept. **301**, 299 (1998).
[75] H. J. Melosh, Quarks: Currents and constituents, Phys. Rev. D **9**, 1095 (1974).
[76] B.-W. Xiao, X. Qian, and B.-Q. Ma, The Kaon form-factor in the light cone quark model, Eur. Phys. J. A **15**, 523 (2002).
[77] W. Jaus, Relativistic constituent quark model of electroweak properties of light mesons, Phys. Rev. D **44**, 2851 (1991).
[78] S. J. Brodsky, T. Huang, and G. P. Lepage, Hadronic wave functions and high momentum transfer interactions in quantum chromodynamics, Conf. Proc. C **810816**, 143 (1981).
[79] S. J. Brodsky, T. Huang, and G. P. Lepage, The hadronic wave function in quantum chromodynamics, Report No. SLAC-PUB-2540, SLAC, Stanford, CA, 1980, https://cds.cern.ch/record/125086.
[80] S. J. Brodsky, T. Huang, and G. P. Lepage, Hadronic and nuclear interactions in QCD, Springer Tracts Mod. Phys. **100**, 81 (1982).
[81] P. Chung, F. Coester, and W. Polyzou, Charge form factors of quark-model pions, Phys. Lett. B **205**, 545 (1988).
[82] F. Coester and W. N. Polyzou, Charge form factors of quark-model pions, Phys. Rev. C **71**, 028202 (2005).
[83] H.-M. Choi and C.-R. Ji, Kaon electroweak form-factors in the light front quark model, Phys. Rev. D **59**, 034001 (1999).
[84] H.-M. Choi, C.-R. Ji, and L. S. Kisslinger, Light front quark model analysis of rare B—> K l+ l- decays, Phys. Rev. D **65**, 074032 (2002).
[85] H.-M. Choi and C.-R. Ji, Distribution amplitudes and decay constants for (pi, K, rho, K*) mesons in light-front quark model, Phys. Rev. D **75**, 034019 (2007).
[86] H.-M. Choi, C.-R. Ji, Z. Li, and H.-Y. Ryu, Variational analysis of mass spectra and decay constants for ground state pseudoscalar and vector mesons in the light-front quark model, Phys. Rev. C **92**, 055203 (2015).
[87] N. Dhiman, H. Dahiya, C.-R. Ji, and H.-M. Choi, Twist-2 pseudoscalar and vector meson distribution amplitudes in light-front quark model with exponential-type confining potential, Phys. Rev. D **100**, 014026 (2019).
[88] B. Pandya, B. Gurjar, D. Chakrabarti, H.-M. Choi, and C.-R. Ji, Mixing effects on spectroscopy and partonic observables of heavy mesons with logarithmic confining potential in a light-front quark model, Phys. Rev. D **110**, 094021 (2024).
[89] R. Acharyya, S. Puhan, H. Dahiya, and N. Kumar, Spectroscopy of excited quarkonium states in the light-front quark model*, Chin. Phys. C **49**, 023104 (2025).
[90] M. V. Terentev, On the structure of wave functions of mesons as bound states of relativistic quarks, Sov. J. Nucl. Phys. **24**, 106 (1976).
[91] J. Carbonell, B. Desplanques, V. A. Karmanov, and J. F. Mathiot, Explicitly covariant light front dynamics and relativistic few body systems, Phys. Rep. **300**, 215 (1998).

[92] V. Karmanov, Relativistic deuteron wave function on the light front, Nucl. Phys. **A362**, 331 (1981).
[93] W. Jaus, Covariant analysis of the light front quark model, Phys. Rev. D **60**, 054026 (1999).
[94] Y. Li, P. Maris, and J. Vary, Frame dependence of form factors in light-front dynamics, Phys. Rev. D **97**, 054034 (2018).
[95] V. A. Karmanov, The wave functions of relativistic bound systems, Sov. Phys. JETP **44**, 210 (1976).
[96] X. Cao, Y. Li, and J. P. Vary, Forces inside a strongly-coupled scalar nucleon, Phys. Rev. D **108**, 056026 (2023).
[97] X. Cao, S. Xu, Y. Li, G. Chen, X. Zhao, V. A. Karmanov, and J. P. Vary, Energy momentum tensor on and off the light cone: Exposition with scalar Yukawa theory, J. High Energy Phys. 07 (2024) 095.
[98] X. Cao, Y. Li, and J. P. Vary, Dissecting a strongly coupled scalar nucleon, Phys. Rev. D **110**, 076025 (2024).
[99] S. Godfrey and N. Isgur, Mesons in a relativized quark model with chromodynamics, Phys. Rev. D **32**, 189 (1985).
[100] B. Bakamjian and L. H. Thomas, Relativistic particle dynamics. II, Phys. Rev. **92**, 1300 (1953).
[101] B. D. Keister and W. N. Polyzou, Relativistic Hamiltonian dynamics in nuclear and particle physics, Adv. Nucl. Phys. **20**, 225 (1991).
[102] A. J. Arifi, H.-M. Choi, C.-R. ji, and Y. Oh, Mixing effects on 1S and 2S state heavy mesons in the light-front quark model, Phys. Rev. D **106**, 014009 (2022).
[103] A. Dwibedi, S. Puhan, S. Ghosh, and H. Dahiya, Distribution functions of radially excited pion using the light-front quark model, arXiv:2601.06628.
[104] W. Jaus, Semileptonic Decays of B and d mesons in the light front formalism, Phys. Rev. D **41**, 3394 (1990).
[105] H.-Y. Cheng, C.-Y. Cheung, and C.-W. Hwang, Mesonic form-factors and the Isgur-Wise function on the light front, Phys. Rev. D **55**, 1559 (1997).
[106] R. G. Sachs, High-energy behavior of nucleon electromagnetic form factors, Phys. Rev. **126**, 2256 (1962).
[107] M. Burkardt, Impact parameter dependent parton distributions and off forward parton distributions for $\zeta \to 0$, Phys. Rev. D **62**, 071503 (2000); Phys. Rev. D **66**, 119903(E) (2002).
[108] G. A. Miller, Defining the proton radius: A unified treatment, Phys. Rev. C **99**, 035202 (2019).
[109] R. L. Jaffe, Ambiguities in the definition of local spatial densities in light hadrons, Phys. Rev. D **103**, 016017 (2021).
[110] C. Lorcé and P. Schweitzer, Pressure inside hadrons: Criticism, conjectures, and all that, Acta Phys. Pol. B **56**, 3 (2025).
[111] I. A. Perevalova, M. V. Polyakov, and P. Schweitzer, On LHCb pentaquarks as a baryon-$\psi(2S)$ bound state: Prediction of isospin-$\frac{3}{2}$ pentaquarks with hidden charm, Phys. Rev. D **94**, 054024 (2016).
[112] J. Hudson and P. Schweitzer, D term and the structure of pointlike and composed spin-0 particles, Phys. Rev. D **96**, 114013 (2017).
[113] S. Puhan, S. Sharma, N. Kumar, and H. Dahiya, Understanding the valence quark structure of the pion through generalized transverse momentum-dependent parton distributions, Prog. Theor. Exp. Phys. **2025**, 083B02 (2025).
[114] S. Puhan and H. Dahiya, Scalar, vector, and tensor form factors of pion and kaon, Phys. Rev. D **111**, 114039 (2025).
[115] N. Li, C.-C. Liu, and Y.-J. Wu, Lattice study of form factors for charmonium, Eur. Phys. J. A **56**, 242 (2020).
[116] Y. Chen *et al.*, Radiative transitions in charmonium from $N_f = 2$ twisted mass lattice QCD, Phys. Rev. D **84**, 034503 (2011).
[117] J. Delaney, C. E. Thomas, and S. M. Ryan (Hadron Spectrum Collaboration), Radiative transitions in charmonium from lattice QCD, J. High Energy Phys. 05 (2024) 230.
[118] S. Borsányi, Z. Fodor, J. N. Guenther, R. Kara, S. D. Katz, P. Parotto, A. Pásztor, C. Ratti, and K. K. Szabó, Lattice QCD equation of state at finite chemical potential from an alternative expansion scheme, Phys. Rev. Lett. **126**, 232001 (2021).
[119] S. Kumano, Q.-T. Song, and O. V. Teryaev, Hadron tomography by generalized distribution amplitudes in pion-pair production process $\gamma^*\gamma \to \pi^0\pi^0$ and gravitational form factors for pion, Phys. Rev. D **97**, 014020 (2018).
[120] G. P. Lepage and S. J. Brodsky, Exclusive processes in perturbative quantum chromodynamics, Phys. Rev. D **22**, 2157 (1980).